CHAPTER 3

DETERMINATION OF TALC'S SURFACE FREE ENERGIES FROM CONTACT ANGLES MEASURED ON FLAT AND POWDERED SAMPLES

3.1- Surface free energy: definition

The atoms at the surface of a condensed-phase material are in a very different environment compared to those atoms from its interior. This difference arises from the asymmetrical environment; in the bulk material, each atom is surrounded by similar ones and they experience no net forces. However, those at the surface see this only on one side of the interface. In addition, the various influencing factors exerted by the environment act only on the outermost atoms [1]. These atoms, consequently, have a different energy distribution from the inside, and are in a higher energy state at the surface. This energy excess is what one wants to measure. Differences between the energies of atoms or molecules located at the surface and in the bulk of a material manifest themselves as surface tension (or surface free energy), γ. The surface free energy of a non-metallic material always has an apolar component (γ^{LW}) and may have a polar component (γ^{AB}) [2].

Qualitatively, surface tension acts in any surface, trying to minimize the surface area, i. e., it is a contractile force. Thus, it is a measure of the tendency of all areas to become as small as possible.

Thermodynamically, the surface tension, γ, is interpreted as the increase in the Gibbs energy of the system when the area of the interface under consideration is increased reversibly by an infinitesimal amount dA at constant temperature (T), pressure (p) and composition (n) [3]. This can be expressed as:

$$\gamma = \left(\frac{\partial G}{\partial A} \right)_{T,p,n_i} \tag{3.1}$$

In other words, surface tension can also be interpreted as the reversible work required to extend a surface or to bring atoms from the interior to the surface region [2].

The terms surface energy and surface tension are being used interchangeably in current literature. However, Good [4] emphasized the importance of the distinction between the two terminologies. Although either of the two terms may be appropriate for use in the case of liquids, for solids the term “surface energy” should bear more physical significance than the term “surface tension” because of the fact that an increase in the surface area of a solid cannot be accomplished without doing work against the elastic forces and plastic resistance of the solid (see Section 3.5 for additional information).

There is now a wealth of spectroscopic and other analytical techniques for probing the surface properties of solid materials [5, 6], which yield a variety of surface properties of those parts of such materials that are situated anywhere between 1.0 and more than 10 nm below their surfaces [7]. However, to date only contact angle analysis is capable of yielding the actual surface or interfacial properties at the precise surface of solids, that are relevant to their interaction with other condensed phase materials [1] and to the purpose of this investigation.

3.2- The Young’s equation

Contact angle (θ) measurement, first stated in qualitative form by Thomas Young in 1805 [8], remains at present the most accurate method for determining the interaction energy between a liquid (L) and a solid (S). Considering, for example, a process in which a liquid drop is brought to the surface of a solid previously in contact with air (V) (see Figure 3.2). The angle measured between the solid surface and the liquid drop, through the liquid phase, is referred to as equilibrium contact angle. Young's

paper contained no mathematical equations whatsoever, but its text expresses clearly Young's proposition as follows:

$$\gamma_{LV} \cos\theta = \gamma_{SV} - \gamma_{SL} \tag{3.2}$$

where γ_{LV}, γ_{SV} and γ_{SL} represent the interfacial energies at the liquid-vapor, solid-vapor and solid-liquid interfaces, respectively.

The derivation of the Young's equation assumes that the solid surface is smooth, homogeneous and rigid; it should also be chemically and physically inert with respect to the liquids to be employed. Ideally, a unique contact angle is expected for a given system, according to Young's equation [9].

3.3- The equilibrium spreading pressure

One suspected source of heterogeneity that could occur with even the most homogeneous surface is the heterogeneity caused by the deposition of molecules emanating from the contact angle liquid, via the gaseous phase, by re-condensation [1]. One school of thought, initiated by Bangham and Razouk in 1937 [10], has it that this condensation of liquid from the contact angle liquid gives rise to complete wetting of the solid surface (see Figure 3.2), which seriously reduces the contact angle. In view of this wetting effect, Bangham and Razouk introduced the terms γ_{LV} and γ_{SV} (for liquid-vapor and solid-vapor). This nomenclature has been followed by many workers in the field of colloid and surface science and was adopted in Equation (3.2).

When the solid surface is in equilibrium with the liquid vapor, the reduction of the surface free energy of the solid to the vapor adsorption is termed the equilibrium spreading pressure, π_e, and hence its addition into Equation (3.2) leads to following form of the Young's equation [11]:

$$\gamma_S = \gamma_{LV} \cos\theta + \gamma_{SL} + \pi_e \tag{3.3}$$

where $\pi_e = \gamma_S - \gamma_{SV}$. Thus, the reduction in the value of the ideal surface free energy of a solid (γ_S) due to the adsorption of liquid vapor onto the solid surface can be measured as a function of π_e.

However, for low energy, homogeneous, smooth surfaces, the approximation that the term π_e is not significant is a reasonable one [12, 13]. Wu demonstrated that on a low energy surface π_e is usually negligible if the contact angle is larger than 10^o [14]. Yildirim experimentally determined that the change in the contact angle of water by exposing talc to water vapor was negligible [11], which indicated that the vapors of high-energy water did not adsorbed onto the low-energy talc surface. Fowkes *et al*. [15] studied the possibility of spreading pressures arising with high-energy liquids (e.g. water vapor) deposited on low-energy solids, and found that it did not occur. On the other hand, when the vapor of a low-energy liquid (e.g. cyclohexane or heptane) could interact with a somehow higher-energy solid surface, the effect of resulting positive spreading pressure caused an increase in the contact angle of water on that solid surface, which allowed the determination of π_e.

By conducting thin layer wicking measurements, van Oss [16] showed that with non-spreading liquids (i.e. $\gamma_L > \gamma_S$ and $\cos\theta < 1$) neither spreading nor pre-wetting takes place on low-energy solid surfaces. Thus, he concluded that it appeared not to be justified to take the equilibrium spreading pressures into account, under non-spreading conditions and where vapors of low energy substances were absent.

In another work, van Oss *et al.* [17] studied on both moderately hydrophobic and very hydrophilic solids, poly(methyl methacrylate) and poly(ethylene oxide), respectively and showed that in virtually all cases the contamination of the surface by gas molecules emanating from the liquid drop could be safely neglected since the error introduced by the effect of the spreading pressure was in the same order of magnitude of the precision of the contact angle measurements (±1%). In conclusion, van Oss [1] suggested that the designations "γ_{LV}" and "γ_{SV}" instead of the simpler γ_L and γ_S are superfluous and misleading and thus are best avoided.

In the light of above statements, Young's equation can then be rewritten in a simpler form as:

$$\gamma_S = \gamma_L \cos\theta + \gamma_{SL} \tag{3.4}$$

where γ_S is the surface free energy of the solid, γ_L is the surface free energy of the testing liquid and γ_{SL} is the surface free energy of the interface solid/liquid. In this form of Young's equation the spreading pressure, π_e, is neglected [18].

3.4- The Young-Dupré equation as a force balance

Historically, the next development (after Young) was due to Dupré, who introduced the concepts of work of cohesion, W^{coh}, and work of adhesion, W^{adh}. While these symbols are still used, there is a considerable advantage in employing thermodynamic notation, in terms of free energy, G, in order to emphasize the fact that γ is, physically, the free energy per unit area, as well as force per unit length, and also to keep the signs of the physical quantities straight [13].

Considering the reversible process of bringing together two cylinders of a condensed-phase material initially in vacuum, to form a continuous body (Figure 3.1), the free energy change per unit area is the free energy of cohesion, ΔG_{ii}^{coh} or the negative of the work of cohesion, $-W_{ii}^{coh}$. For this process,

$$\Delta G_{ii}^{coh} = -2\gamma_i = -W_{ii}^{coh} \tag{3.5}$$

As an approximation, the initial surfaces, which are destroyed in the process, may be taken to be between the condensed phases and vacuum.

When two unlike bodies are brought together reversibly, the free energy change per unit area is the free energy of adhesion, ΔG_{ij}^{adh}, or the negative of the work of adhesion, $-W_{ij}^{adh}$ (see Figure 3.1). For this process,

$$\Delta G_{ij}^{adh} = \gamma_{ij} - \gamma_i - \gamma_j = -W_{ij}^{adh} \tag{3.6}$$

where γ_i and γ_j refer respectively to phase *i* and phase *j* in vacuum, i.e. in equilibrium with their own vapor [19], and *ij* refers to the *ij* interface.

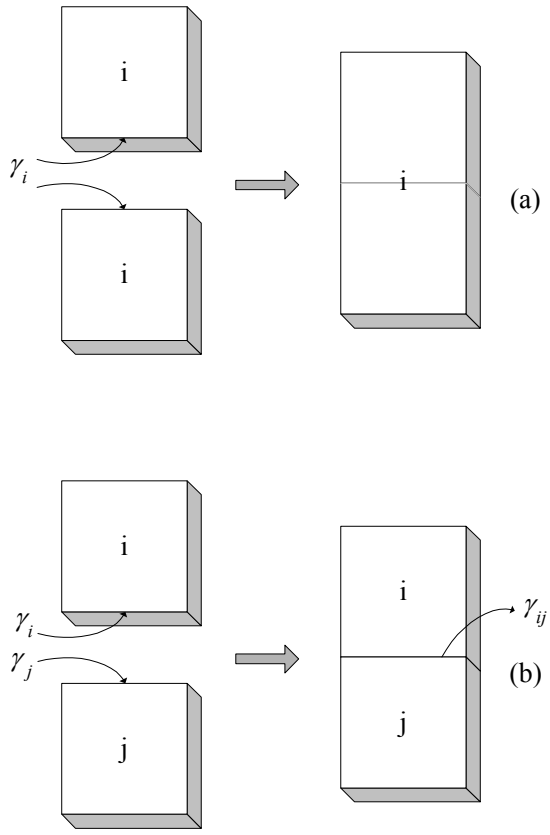

Figure 3.1 - Diagram illustrating the thermodynamic cohesion process (Eq. 3.5). (b) Diagram illustrating the thermodynamic adhesion process (Eq. 3.6). From ref. [13].

Recalling Eq. (3.4), the surface free energy of the testing liquid, γ_L, and $\cos\theta$ are known and γ_S and γ_{SL} are the unknowns. Using two different liquids gives rise to two equations with three unknowns, i.e., γ_S, γ_{SL1}, and γ_{SL2}, where the subscripts 1 and 2 refer

to the two equations (i.e., the two different liquids). Thus, Eq. (3.4), in the form given above, is not practically usable when attempting to determine the surface free energy of a given solid.

However, in conjunction with the Dupré equation (Eq. (3.6)) in the following form:

$$\Delta G_{SL}^{adh} = \gamma_{SL} - \gamma_S - \gamma_L \tag{3.7}$$

which is the change in free energy associated with the liquid drop-solid adhesion process, Eq. (3.4) becomes:

$$(1+\cos\theta)\gamma_L = -\Delta G_{SL}^{adh} \tag{3.8}$$

which is known as the Young-Dupré equation. Equation (3.8) has only one unknown - ΔG_{SL}^{adh}. The change of free energy of the liquid drop due to deformation is equal to the free energy change due to adhesion of the liquid with the solid. The Young-Dupré is a mathematical representation of the above statement.

Combining Eq. (2.51) (Chapter 2) with Eq. (3.8) one obtains:

$$\frac{1+\cos\theta}{2}\gamma_L = \sqrt{\gamma_S^{LW}\gamma_L^{LW}} + \sqrt{\gamma_S^{\oplus}\gamma_L^{\ominus}} + \sqrt{\gamma_S^{\ominus}\gamma_L^{\oplus}} \tag{3.9}$$

which is known as van **O**ss-**C**haudhury-**G**ood (OCG) thermodynamic approach to determine the values of surface free energy components of solids, applicable to apolar as well as to polar systems [16, 20, 21]. In Eq. (3.9) the left hand side (containing the contact angle θ, measured through the aqueous phase, at the tangent to the drop) represents the part of the energy of cohesion of the liquid[1], L, which is in equilibrium

[1] Which tends to make the drop maintain the spherical shape.

with and therefore equal to, the energy of adhesion[2] between liquid, L, and solid, S, expressed in the right side of Eq. (3.9). Therefore, the value of contact angle θ is a measure of the competing tendencies between the energy of cohesion of the liquid molecules and the energy of adhesion between liquid and solid [11]. When the energy of cohesion between liquid molecules exceeds the energy of adhesion between solid and liquid, a drop of liquid placed on the solid surface forms a finite (non-zero) contact angle. On the contrary, if the energy of adhesion is higher than the energy of cohesion spreading occurs.

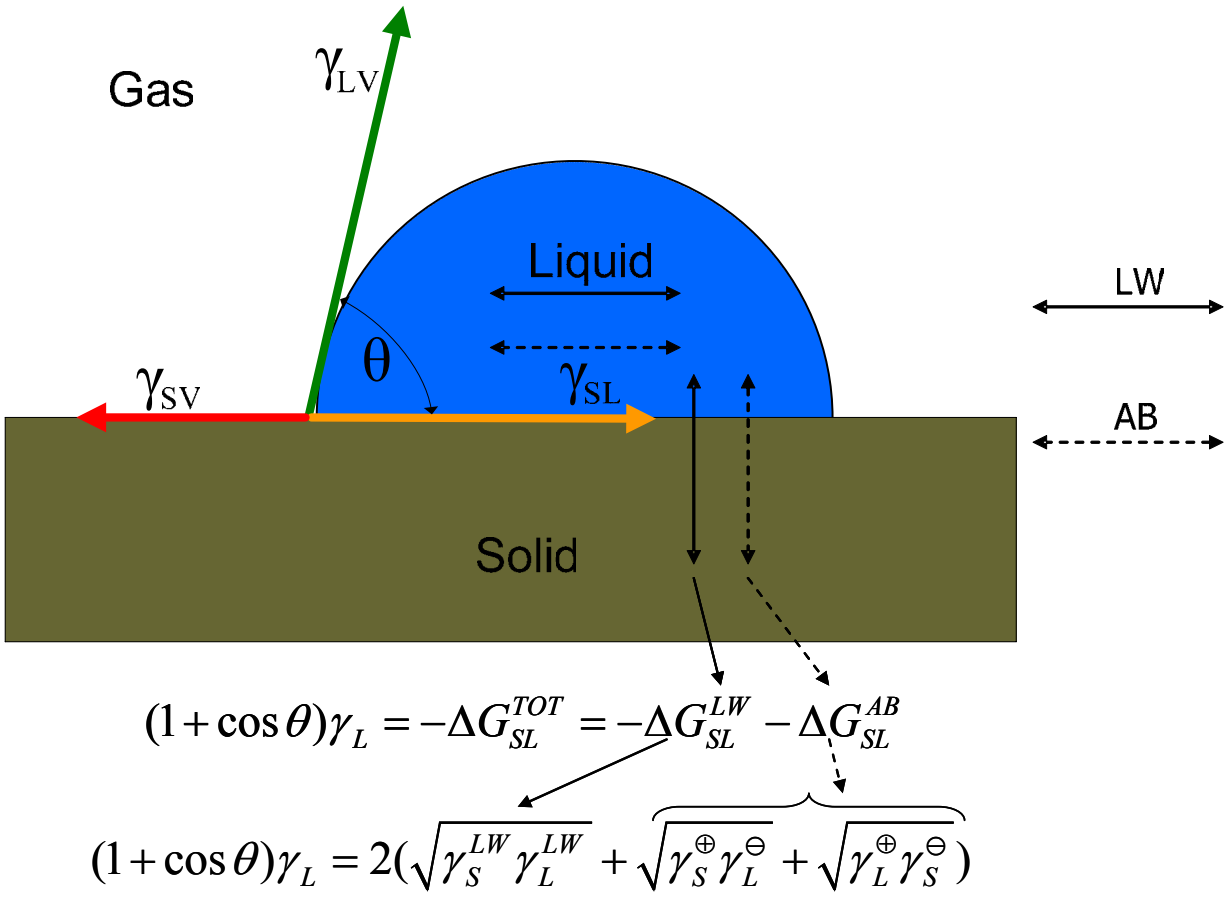

Figure 3.2 - The contact angle, θ, as a force balance. Cosine θ is a measure of the equilibrium between the energy of cohesion between the molecules of liquid L (horizontal arrows; left-hand side of the equation) and the energy of adhesion (vertical arrows; right-hand side) between liquid L and solid S. The solid lines represent apolar interactions and dashed lines are polar interactions. Adapted from ref. [16].

[2] Which tends to flatten the drop.

It should be emphasized that Figure 3.2 also illustrates the importance of acid-base interactions on the value of contact angle, hence on the magnitude of adhesion. Thus, the measured contact angle between L and S permits the use of the liquid-solid interaction as a force balance. It should be noted that Eq. (3.9) contains three unknowns, i.e., γ_S^{LW}, $\gamma_S^{\oplus}$ and $\gamma_S^{\ominus}$ (assuming that the values for γ_L^{LW}, $\gamma_L^{\oplus}$ and $\gamma_L^{\ominus}$ are known as they would be in a real experiment). To obtain the three γ-component values for the solid, S, it is therefore necessary to measure contact angles with three different liquids, L_1, L_2, and L_3, of which at least two must be polar.

If an apolar liquid is placed on the surface of a talc sample and its contact angle is measured, Eq. (3.9) can be reduced to:

$$\left(1+\cos\,\theta\right)\gamma_L = 2\sqrt{\gamma_S^{LW}\gamma_L^{LW}} \tag{3.10}$$

because $\gamma_L^{\oplus}$ and $\gamma_L^{\ominus}$ are zero. Thus, Eq. (3.10) can be used to determine γ_S^{LW} from a single contact angle value, if the contact angle measurement is conducted with an apolar liquid of known γ_L and γ_L^{LW} (in fact, for an apolar liquid γ_L = γ_L^{LW} since $\gamma_L^{\oplus}$ and $\gamma_L^{\ominus}$ are zero). Having determined γ_S^{LW}, the next step is to conduct contact angle with two different polar liquids, e.g. water and formamide. In this case, Eq. (3.9) can be solved to determine the values of $\gamma_S^{\oplus}$ and $\gamma_S^{\ominus}$ by solving two rather than three simultaneous equations.

Once the three surface tensions, i.e., γ_S^{LW}, $\gamma_S^{\oplus}$ and $\gamma_S^{\ominus}$, are known, one can use Eqs. 2.33 and 2.38 to determine the total surface tension of the solid, γ_S^{Total}, as follows:

$$\gamma_S^{Total} = \gamma_S^{LW} + 2\sqrt{\gamma_S^{\oplus}\gamma_S^{\ominus}} \tag{3.11}$$

A list of the most used contact angle liquids, with their γ-properties at 20°C, is given in Table 3.1.

It should be emphasized that, to obtain finite, measurable contact angles γ_L must be greater than γ_S. When $\gamma_L < \gamma_S$, the liquid forms no contact angle on the solid, but spreads and wets it completely. In other words, the extent of partial wetting of the solid by the liquid is quantified by the value of θ: the better the wetting, the lower is θ. Examples of poorly wetting systems are mercury on glass and water on hydrophobic surfaces, where one can see little liquid drops that may roll over the surface. At the opposite extreme, complete wetting occurs when the liquid fully covers the solid. In that case, the liquid spreads spontaneously over the surface and no contact angle can be defined [3].

Thus, it is natural at this point to introduce the definition of the spreading coefficient [22, 23]:

$$S = \gamma_S - (\gamma_{SL} + \gamma_L) \tag{3.12}$$

The spreading coefficient is a measure of the difference in surface energy between the bare dry solid and the moist solid covered by macroscopic film of liquid. If S ≥ 0, spreading occurs (complete wetting) or, in other words, the work of adhesion is higher than the work of cohesion. When S is negative, the surface prefers to remain dry, which is the situation in partial wetting. The liquid will only spread to cover part of the solid and in equilibrium will assume a finite contact angle. In both cases, the total free energy of the system is minimized. The work of Rowe [24] and Buckton [25] exemplifies the practical application of spreading coefficient in, for example, the pharmaceutical field. Using Equations (3.5) and (3.6), one can relate the spreading coefficient to the work of adhesion and cohesion so that for the liquid L on solid S:

$$S = W_{SL}^{adh} - W_{LL}^{coh} \tag{3.13}$$

As a final word, it is worth to mention that the water contact angle can be taken as a measure of the relative hydrophilicity or hydrophobicity of a given solid [9, 11, 26], i.e., the higher the contact angle is, the more hydrophobic the solid surface becomes. In principle, solids having lower surface free energies (γ_S) exhibit higher values of water contact angles. Figure 3.3a illustrates a water drop showing a contact angle of 174^o on a very hydrophobic surface, whereas Figure 3.3b illustrates a surface less hydrophobic (θ = 109^o) and the new equilibrium shape adopted by the water drop [27].

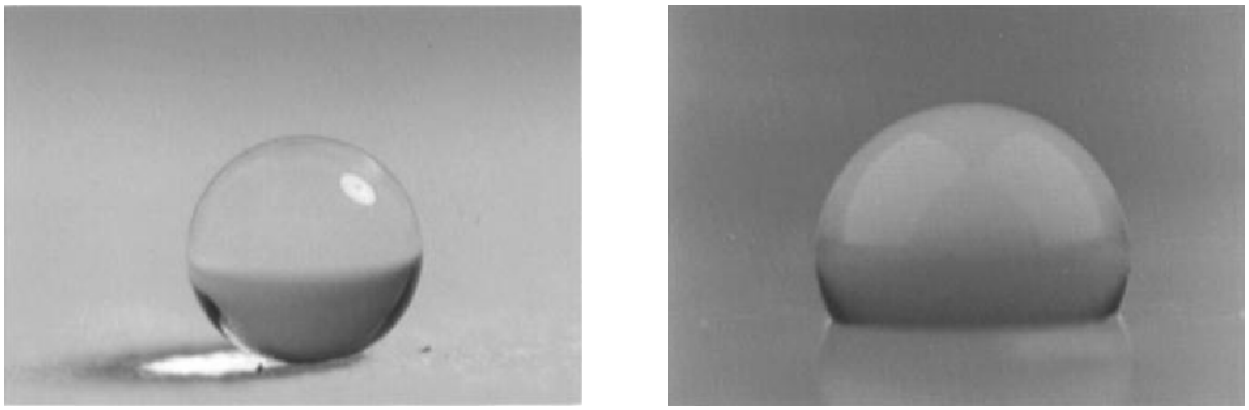

Figure 3.3 - Drop of water on an alkylketene dimmer surface: (a) very hydrophobic surface; (b) less hydrophobic surface. Reprinted with permission from ref. [27]. Copyright 1996 American Chemical Society.

Table 3.1. Surface tension components and parameters of liquids useful for contact angle and wicking measurements, at 20^{o}C, in mJ/m^2, and their viscosities, in poises. From ref. [16]

Liquid	γ^{TOTAL}	γ^{LW}	γ^{AB}	$\gamma^{\oplus}$	$\gamma^{\ominus}$	η
Apolar						
Hexane	18.4	18.4	0	0	0	0.00326
Octane	21.62	21.62	0	0	0	0.00542
Nonane	22.85	22.85	0	0	0	0.00712
Decane	23.83	23.83	0	0	0	0.00907
Undecane	24.65	24.64	0	0	0	0.01191
Dodecane	25.35	25.35	0	0	0	0.01493
Tetradecane	26.6	26.6	0	0	0	0.02180
α-bromonaphthalene	44.4	44.4	0	0	0	0.0489
Diiodomethane	50.8	50.8	0	0	0	0.028
Polar						
Water	72.8	21.8	51.0	25.5	25.5	0.010
Formamide	58	39	19	2.28	39.6	0.0376

3.5- Surface heterogeneity: contact angle hysteresis

When a liquid advances over a solid surface, the angle thus observed in called the advancing contact angle, θ_a. Contrary, the angle observed when the liquid recedes from the surface is called the receding or retreating contact angle, θ_r [12].

Hysteresis is ordinarily defined as the difference between the advancing and retreating angles [4]:

$$H \equiv \theta_a - \theta_r \tag{3.14}$$

The common terms, “advancing angle” for θ_a and “receding angle” for θ_r, are misleading in that they give the impression that measurement is made while advance or retreat is in progress. In fact, they are measured when an advancing or a receding liquid front over a solid is stopped. Then a constant angle is attained in a short time [4].

There are a number o more or less independent causes of hysteresis. Two major causes are surface roughness and surface chemical heterogeneity [28, 29]. Adamson [30] pointed out various other possible causes for hysteresis such as solution impurities adsorbing on the surface, or swelling, rearrangement or alteration of the surface by the solvent. For ideally smooth and homogenous solid surfaces, the values of θ_a and θ_r should be very close [31]. However, the difference between θ_a and θ_r can be quite large, as much as 50^o for water on mineral surfaces, suggesting surface heterogeneity.

It has been suggested that both advancing and retreating contact angles should be measured wherever possible. Because, there is likely to be chemical information residing in retreating contact angle data that is different from the information in advancing contact angles for the same solid surface [11, 13, 18].

As a result of the analysis of Good and Neumann, it has been established that for smooth, heterogeneous solids the advancing contact angle corresponds approximately

to Young's equilibrium contact angle associated with low energy patches of the surface, whereas the receding contact angle corresponds to that of high energy patches [12]. Whilst advancing contact angles (θ_a) have been held to be a measure of the apolar aspect of a surface, and receding contact angles (θ_r) a measure of the polar aspects of the solid [16], it would be hazardous to take that statement so literally as to attempt to derive the polar surface tension component of the solid by measuring θ_r.

Methods have been worked out for applying correction factors to the measured (advancing) contact angles, once the radius of roughness has been determined [12]. However, using smooth surfaces, i.e., surface with radii of roughness significantly smaller than 1 μm, is by far preferable [12].

Usually hysteresis, when it occurs, is positive, i.e., $\theta_a > \theta_r$, indicative of complete or partial residual wetting of the solid surface by the liquid of the retreating drop. However, negative hysteresis (i.e., $\theta_a < \theta_r$), although rare, can take place [1].

It is generally assumed that the experimental advancing contact angle can be expected to be a good approximation of the Young's contact angle [32]. Therefore, care must be taken to ensure that the experimental apparent contact angle is the advancing contact angle in order to be inserted into the Young's equation.

The much more common occurrence of positive contact angle hysteresis with polar liquids (e.g., with water) on polar surfaces is caused by the residual wetting the retreating liquid leaves behind. Thus, only the advancing contact angle (θ_a) has significance when used to obtain γ-values by means of the Young-Dupré equation (Eq. (3.9)), because only an advancing drop encounters a new uncontaminated surface. The angle made by a receding drop has no quantitative significance in conjunction with Eq. (3.9), and may only offer an exceedingly rough qualitative indication of surface roughness, heterogeneity or partial hydrophilicity [1].

3.6- Experimental methods to determine contact angle of solids

As has already been discussed, it is necessary to measure the contact angle (θ), if one whishes to characterize the surface of a solid in terms of its surface free energy components, i.e. γ_S^{LW}, $\gamma_S^{\oplus}$ and $\gamma_S^{\ominus}$. There are several different methods that have been developed for measuring contact angles. The classic techniques have been reviewed in detail by Neummann and Good [33] and the most used are summarized in the following section. The choice of a particular method depends on which geometry of the solid of interest is available, i.e. as a flat plate, as a fiber, in the powdered form, etc. Direct methods such as sessile drop and captive bubble techniques are widely used for the flat surfaces. The Wilhelmy plate technique and the Wilhelmy gravitational method are used to determine the advancing and receding contact angles on the flat (or plate) surfaces and fibers, respectively. For powders, the methods based on wicking, i.e. column wicking and thin layer wicking, are among the most used. The calorimetric technique (heat of immersion) is also applicable to powders and is briefly described.

3.6.1- Direct measurements: flat surfaces

3.6.1.1- Sessile drop or adhering gas bubble (captive bubble)

The direct measurement of angle from drop profile by using either the sessile drop or, alternatively, the captive bubble technique is at present the most widely used method. It is, in general, the most convenient method if high accuracy is not required, and it has the two great advantages of requiring only very small quantities of both liquid and solid surface. The main drawback of this method is that it is subjective and the results depend on the experience of the operator. Although certain training procedures can be used to improve the reproducibility, the accuracy of this method is usually $\pm 2^o$ [9, 33].

In the sessile drop technique, a liquid droplet is placed on the surface of the solid and the contact angle is measured simply by aligning a tangent to the drop profile at the

point where the three interfaces meet, i.e. the base of drop. Commercial contact angle goniometers employ a microscope objective to view the angle directly at the tangential line formed between the solid surface and the sessile drop. More sophisticated approaches involve a photograph or digital image of the drop profile [30]. When high accuracy is needed, a more advanced method, the Axisymmetric Drop Shape Analysis (ADSA), developed by Neumann can be employed. In the ADSA methodology, images of a drop or a bubble are acquired, and the contact angle is determined by a computer program that fits an equation to the drop/bubble profile. A standard deviation of $\pm 0.2^{o}$ can be achieved by ADSA [9, 34-37].

In order to establish advancing and receding contact angles of a sessile drop, liquid is slowly injected into or withdrawn from a drop by means of a syringe assembly.

In the captive bubble technique, the solid is immersed on the surface of a liquid and an air bubble (or drop of another liquid) is brought to the solid/liquid interface. The angle between the surface of the solid and the air bubble is then measured through the liquid phase from either photographs of the bubble profile, or directly, by means of a goniometer telemicroscope. The main advantage of this technique is that it minimizes the effect of adventitious contamination [30].

3.6.1.2- Capillary rise at a vertical plate

The capillary rise on a vertical plate is another way to obtain contact angles by measurement of the height, *h*, of the meniscus on a partially immersed plate. As shown in Figure 3.4, for a vertical flat plate brought into contact with a pool of liquid, the latter may rise or be depressed near the vertical wall depending on the equilibrium contact angle. For such a capillary rise profile around an infinitely wide flat plate, a relation between the contact angle and the height of the capillary rise can be obtained from [38-41]:

$$1-\sin\theta=\frac{\Delta\rho_{lv}gh^2}{2\gamma_L} \tag{3.15}$$

where $\Delta\rho_{lv}$ is the density difference between the liquid phase and the vapor phase, *g* it he acceleration due to gravity, *h* is the capillary rise height, γ_L is the surface tension of the testing liquid and *θ* is the contact angle of the liquid on the vertical plate. For practical purposes, plates that are about 2 cm wide satisfy the theoretical requirement of "infinite" width and the edge effects can be neglected [33]. One advantage of this technique is that the measurement of an angle has been changed into the measurement of a height that can be implemented much more accurately.

Recently, a new approach of measuring the capillary rise was developed by Neummann and Budziak [42] using digital image analysis in conjunction with high-precision translation stages. An accuracy of $\pm 0.2^o$ was reported.

This method is particularly suitable for measuring the temperature dependence of contact angle [43]. In addition, dynamic advancing and receding contact angles can be measured by moving the plate up or down [33].

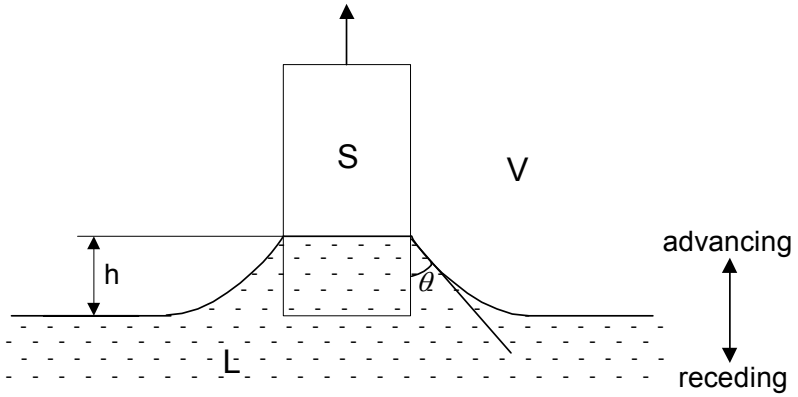

Figure 3.4 - Schematic of capillary rise of a liquid at vertical plate, where θ is the contact angle, and *h* is the capillary rise height. Adapted form refs. [33, 40].

3.6.1.3- The Wilhelmy gravitational method[3]

It was noticed that the capillary rise technique requires a large flat solid surface and hence cannot be used to measure contact angle on a curved surface such as cylindrical fiber surface. However, the measurement of the contact angle or wettability on a natural or artificial fiber is of practical importance in the composite, textile and cosmetic industries [39]. Since the equation for the Wilhelmy technique, Eq. (3.16), do not depend on the geometry of the solid surface, as long as the walls of the solid are parallel and normal to the liquid surface, the method is applicable not only to plates, but also to rods, wires, capillary tubes and fibers [9]. In this method, a solid hanging on an electronic balance is partially immersed in a testing liquid. Thus, the contact angle is determined by measuring the force *f* required to balance the solid [33, 39]:

$$f = p\gamma_L \cos\theta - V\Delta\rho_{lv}g \tag{3.16}$$

where *p* is wetted perimeter of the solid, γ_L is the surface tension of the testing liquid, *θ* is the contact angle of the liquid on the solid, V is the liquid volume displaced by the solid or the volume of the solid immersed in the liquid, $\Delta\rho_{lv}$ is the density difference between the solid phase and the liquid phase and *g* it he acceleration due to gravity.

Figure 3.5 shows a schematic of an experimental set-up for the Wilhelmy gravitational technique. The fiber/plate ①, the perimeter of which should be constant, is suspended by a thin rod ② from the very sensitive electronic balance ③. The downward force is recorded on a computer ④. The testing liquid ⑤ is placed in a beaker. The traveling stage ⑥, controlled by the computer, is moved up and down to determine the advancing and receding contact angles. The system is surrounded by an environmental chamber ⑦ mounted in a vibration-proof platform.

[3] Also known as Wilhelmy balance and Wilhelmy plate technique.

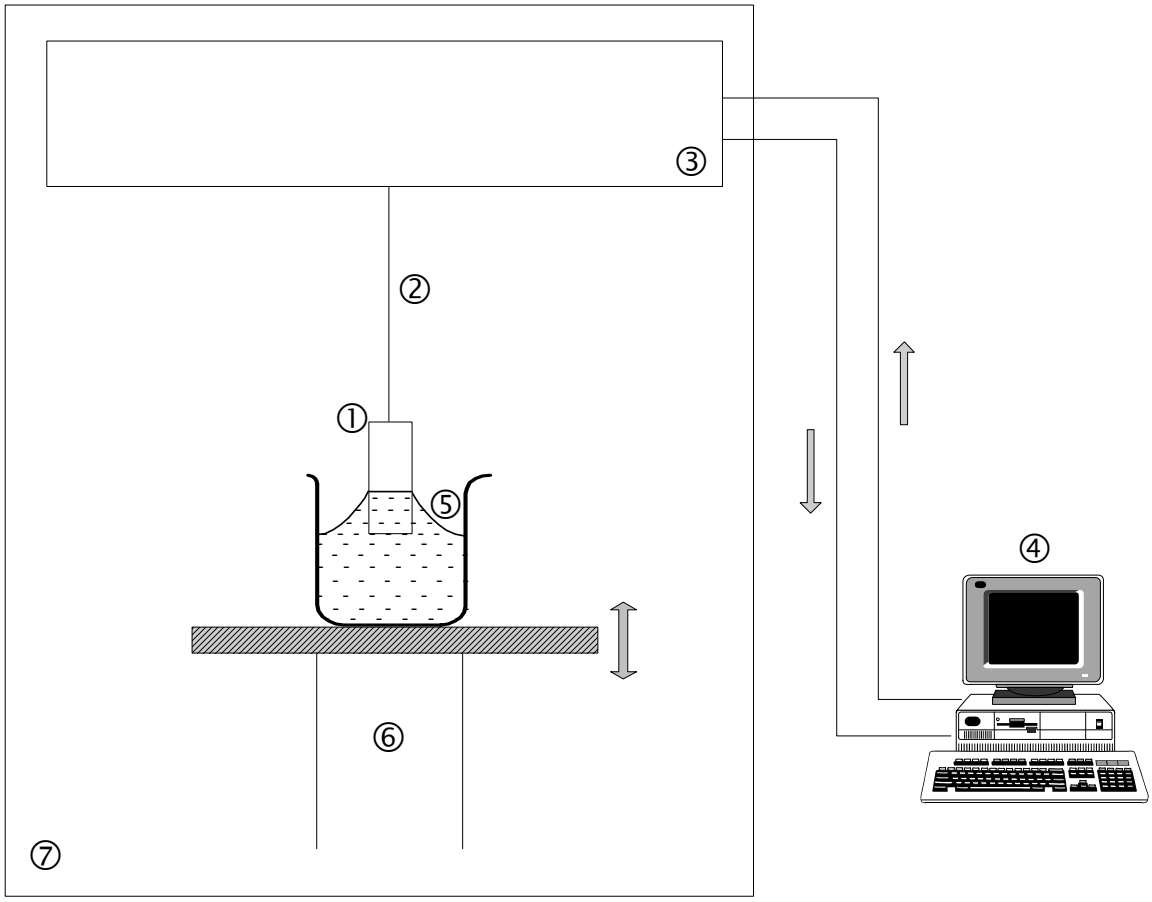

Figure 3.5 - Schematic of the apparatus for the Wilhelmy plate technique: measuring plate ①, rod ②, electronic balance ③, computer ④, testing liquid ⑤, traveling stage ⑥, environmental chamber ⑦. Adapted form ref. [9, 33].

3.6.2- Indirect measurements: powdered solids

Many naturally occurring or artificially obtained solids which are of great practical interest, like soils, clays, pigments, polymers, pharmaceutics, and others, can be obtained only as powders, irregular fibers, microscopic particles and no flat and smooth surface of them can be satisfactorily prepared. For such solids, the contact angle cannot be measured directly and, consequently, none of the above discussed methods can be employed. Indirect methods of obtaining the contact angle must be used [44].

3.6.2.1- Compressed powders

A very common approach to assessing contact angles for powders is to make a compacted disc of powder, which is saturated with the test liquid, and then to observe a drop of the test liquid on the compact surface [45]. The contact angle can then be assessed by any direct measurement technique as described in Section 3.7.1 for flat surfaces. In addition to the particular limitations of the direct methods of contact angle determination, the need to saturate the compacted bed can cause swelling [46], the pellets are usually rough and porous, which causes a smaller contact angle to be measured on the pellet than would be obtained on a smooth specimen of this solid [47] and other problems such as liquid adsorption [11] might appear. Besides, the plastic distortion of the topmost powder particles by the compression is likely to render the exposed surface quite unlike the surface of the uncompressed powder. For these reasons, the measured contact angles on compacted surfaces might significantly differ from those obtained on flat surfaces and they can yield, at the best, qualitative information [33]. The Wilhelmy gravitational technique was also applied by using wafer-like compacts of the test solid [48]. However, it still requires use of compressed powder samples, giving potential for compression associated problems.

3.6.2.2- Chromatographic methods

Other methods applied for determination of powdered solid surface free energy are adsorption gas chromatography and inverse gas chromatography. In adsorption gas chromatography, the free surface energy of the solid is calculated from the adsorption isotherms obtained during the determination of the adsorbate film pressure π. Using adsorbates that interact with the solid surface by the dispersion forces only (like hydrocarbons), or both dispersion and polar forces (like water and alcohols), the dispersion and polar components of the solid surface free energy can be determined [49].

In recent years, the thermodynamic characteristics of solid surfaces have been determined by inverse gas chromatography (IGC) [50-59]. However, obtaining reliable parameters by this technique is rendered difficult by several theoretical and practical problems as discussed by Pukanszky [60, 61]. According to the principle of the method, the column is packed with the solid to be characterized (adsorbent or stationary phase) and probe molecules (adsorbate or mobile phase) with known thermodynamic characteristics are adsorbed onto its surface. Surface characteristics can be derived from retention times or volumes.

To determine the apolar component of the solid surface low molecular weight n-alkanes in gaseous form are used. The acid-base components are assessed by percolating the column with polar probes, e.g. chloroform, ethyl acetate, diethyl ether and tetrahydrofurane. In both cases, the numerical values of the surface parameters are obtained by using appropriate mathematical models. In the author's opinion this method can be used as an alternative or complementary method to the thin layer wicking for the cases when the contact angle is higher than 90^{o} and when the knowledge of the effect of temperature on the surface components is needed.

3.6.2.3- Calorimetry: heat of immersion

Heat of immersion, another indirect approach, is a measure of the wettability of the powder immersed in a liquid. It is defined as the heat evolved per unit area of powder immersed in a liquid. The heat of immersion is a measurable quantity and can be related to contact angle. However, it is not only related to contact angle, but also to the temperature-dependence of the contact angle [9], which is a parameter hard to be obtained experimentally.

The thermodynamics of immersion have recently been reviewed [11, 62-64]. After rigorous thermodynamic considerations, the contact angle can be calculated by using the following equation:

$$\cos\theta = \frac{1}{H_L}\left[\gamma_L T\left(\frac{\partial \cos\theta}{\partial T}\right)_p - \Delta H_i\right] \tag{3.17}$$

where H_L and γ_L are the enthalpy and surface tension of the immersion liquid, respectively and are usually available in the literature. ΔH_i is the specific heat of immersional wetting given in units of mJ/m^2 and can be assessed by using a microcalorimeter.

There are several ways of determining temperature coefficient of $\cos\theta$ [11]. First, one measures θ on polished talc samples as a function of temperature and determine $\partial\cos\theta/\partial T$ experimentally. An assumption made here is that although contact angle may change when it is pulverized, its temperature coefficient may remain the same. Second, the contact angle of a powdered sample is measured by pressing it into a pellet. Again, the pressed sample may have a different contact angle from that of loose powders. However, its temperature coefficient may be assumed to remain the same. Third, the contact angles of powdered samples are measured using the capillary rise technique. This technique gives advancing rather than equilibrium contact angles. If one uses this technique to determine $\partial\cos\theta/\partial T$, an implicit assumption is that the temperature coefficients of the equilibrium and the advancing angles are the same.

Malandrini et al. [65] reported the contact angle values of water on various talc samples obtained from microcalorimetric measurements in the range of 29-59^o at 20^{o}C. Recently, Yildirim [11] obtained a better agreement between the contact angle measurements on various talc powders using the heat of immersion technique and the thin layer wicking. The water contact angles thus obtained were in the range from 66 to 78^o and much closer to other reported values. As far as back as 1936, Bartell and Zuidema [66] measured a high contact angle on a polished talc surface. In 1940, Fowkes and Harkins obtained a very close result [67]. Similar measurements have been reproduced using either the sessile drop [68, 69] or the wicking technique [70]. Michot et al. [71] calculated the contact angle of water on the basal surface of talc from wetting

enthalpy measurements. All contact angle values of water on talc surface were around 80^{o}.

Adamson [30] related the heat of immersion enthalpy which can be readily measured by a microcalorimeter to the contact angle, θ, through the application of Young's equation (Eq. (3.2)) as follows:

$$H_i = -\gamma_L \cos\theta - (\gamma_S - \gamma_{SV}) - T\left(\frac{\partial \gamma_{SL}}{\partial T} - \frac{\partial \gamma_S}{\partial T}\right) \tag{3.18}$$

Since in practice, γ_S-γ_{SV} and $\partial\gamma_S/\partial T$ are negligibly small for systems having large contact angles and also the value of $\partial\gamma_{SL}/\partial T$ assumed to be relatively constant for low energy surfaces, i.e, $\partial\gamma_{SL}/\partial T$=0.07±0.02 mJ m^{-2} K^{-1}, a simple relationship between contact angle and heat of immersion enthalpy can be established as:

$$\cos\theta = \frac{-0.07T - H_i}{\gamma_L} \tag{3.19}$$

Eq. (3.19) has been shown to work well for low energy (nonpolar) solids such as graphon [72], teflon [73], fluorinated hydrocarbons [74] and methylated silica surfaces [75].

At present, however, the methods based on imbibition of solid porous layer by a liquid are seemingly getting increasing interest. One variant of these methods, the so-called thin layer wicking, constitutes the chosen approach for investigation of the surface thermodynamics components of talc in this study. Therefore, more attention will be focused on this method.

3.6.2.4- Contact angle determination using wicking techniques

Small, hard particles and powders, of a diameter of 1 μm or more, when spread into flat layers will form a surface that is too rough for accurate contact angle

measurements by the sessile drop method. This roughness invariably results in measured contact angles that are too high [12]. Porous materials have the same drawback, as have pressed pellets of particles, with the added difficulty that the contact angle liquid tends to disappear into such porous bodies, by capillarity, before they can be properly measured.

However, by using a packed column (column wicking) or film (thin layer wicking) of such particles, the capillary rise velocity measurement of a liquid in that column/film can also yield the contact angle of that liquid with respect to the particles' surface. Thus, now-swelling particles, powders or porous solids can still be used in contact angle measurements, by wicking.

Wicking is the measurement of the (cosine of the) contact angle which liquids make with particulate solids, by determining the rate of capillary rise of these liquids in packed beds of such solid materials [76]. Washburn [77] has described the rate of penetration, ν, of liquid into small cylindrical capillaries, viz.:

$$\nu = \frac{dl}{dt} = \frac{R_{eff}\gamma_L \cos\theta}{4\eta l} \tag{3.20}$$

where l is the depth of liquid penetration, R_{eff} is the effective interstitial pore radius of the bundle of capillaries, γ_L, is the surface tension of the liquid, θ is the contact angle, and η is the viscosity of the testing liquid. For $\theta<90^o$, ν is positive indicating that penetration is spontaneous while for $\theta>90^o$, ν is negative indicating that liquid withdrawal from capillaries is spontaneous. In an integrated form, the Washburn equation is expressed as:

$$h^2 = \frac{tR_{eff}\gamma_L \cos\theta}{2\eta} \tag{3.21}$$

where h is the height to which liquid has risen in time t. One fundamental difficulty of this approach is the fact that one uses one equation (3.21) with two unknowns (R_{eff} and $cos\theta$). This difficulty has been addressed by using a liquid which is expected to spread over the solid material under study, in which case it is held that $cos\theta$ = 1, so that Eq. (3.21) can be solved for R_{eff}. This can be done by using low-energy apolar liquids, in this case heptane, octane, decane and dodecane which completely wet the solid surface without forming a finite contact angle [70]. Thus, the value obtained for R_{eff} can then be used with the same particles to solve for $cos\theta$ obtained with non-spreading liquids (in which case $cos\theta$ < 1). This approach tacitly assumes that when one does wicking with a series of spreading liquids of decreasing surface tension γ_L, the term $\gamma_L cos\theta$ (equation (3.21)) remains equal to γ_L. It can be shown that by using the mentioned spreading liquids, θ remains exactly equal to zero, so that $cos\theta$=1, as the result of the formation of a precursor film that pre-wets the surfaces of the particles over which they subsequently spreads [76].

3.6.2.4.1- Column wicking

In the column wicking technique, a powdered solid is packed into the capillary tubing of very small diameter (1.5 – 2.0 mm), which is subsequently immersed into a liquid of known surface tension. The liquid will rise through the capillaries formed in between the particles within the tubing. The distance traveled by the liquid as a function of time *t* is measured and the contact angle is then obtained by means of the Washburn equation (Eq. (3.21)).

Despite being used frequently on mineral powders [78, 79], some precautions regarding the application of this technique must be highlighted. To use the column wicking approach for the determination of $cos\theta$, it is essential to use exceedingly well-packed columns of rather monodisperse particles [80]. If, upon first contact with an ascending (and lubricating) liquid, tighter packing can occur locally, a gap will be created between particles, which causes a strongly asymmetrical rise of the liquid in the packed column. This makes it very difficult or even impossible to measure the precise length of

travel of the liquid column with any particles that are not perfectly spherical and monodispersed [1, 76].

However, in those cases where only polydisperse suspensions of irregularly shaped particles are available, an extremely useful alternate approach is the coating of such particles onto, e.g., glass surfaces, followed by the measurement of the capillary rise of various liquids L, as outlined above, in the manner of thin layer chromatography. This method, which was first suggested by Dr. M. K. Chaudhury [1], is known as thin layer wicking and is depicted in the next section.

3.6.2.4.2- Thin layer wicking method

In the thin layer wicking method, a powdered sample is deposited on a microscopic glass slide in the form of aqueous slurry on which a thin layer of the powdered mineral has been formed. After drying the sample, one end of the glass slide is immersed vertically or horizontally in a liquid. The liquid will start to penetrate slide through the capillaries formed between the particles deposited on the glass surface. The velocity at which a liquid creeps up the slide is measured, and then converted to a contact angle using the Washburn equation (Eq. (3.21)) [70, 76].

The success of the thin layer wicking procedure rests on the ability to fabricate a series of glass slides covered with uniform thin layers of finely powdered sample. This is usually possible for materials which form stable or nearly stable suspensions in water (the most common medium for minerals). Holysz demonstrated that small variations on the layer thickness do not interfere on the final results [81]. To ensure that the powder remains in suspension, the liquid should be stirred with a magnetic stirrer during the process. The typical glass microscope slide (2.5 x 7.5 cm, or 1" x 3") will support approximately up to 5 ml of aqueous suspension. The number of slides to be prepared for each sample is determined by the number of liquids used and the number of replicates desired. The replicates (more than one slide with the same liquid) allow an

estimate of the uniformity of the sample procedure. The alkanes listed in Table 3.1 can be used to determine the pore radius R_{eff} (Eq. (3.21)).

It is of some advantage to calculate the various parameters in the following order: first, the average effective pore radius R_{eff} obtained from the wicking results with spreading liquids (usually alkanes); and second, the various values of $cos\theta$ to be obtained with non-spreading liquids. The γ_S^{LW} value can be derived by wicking with apolar (or virtually apolar) liquids which form a finite contact angle, using Eq. (3.9) without the $\gamma^{\oplus}$ and $\gamma^{\ominus}$ terms (α-bromonaphthalene and diiodomethane); finally, the polar parameters $\gamma_S^{\oplus}$ e and $\gamma_S^{\ominus}$ are obtained by wicking with polar liquids (water and formamide) using the γ_S^{LW} value obtained earlier and Eq. (3.9).

Having determined values of h^2/t for the spreading liquids (usually 3-6 n-alkanes), one plots $2\eta h^2/t$, the so-called wicking coefficient, versus γ_L, for each liquid and determine the least squares straight line that passes through both the origin and the spreading liquid data points. The slope of this line is the average pore radius, R_{eff}. This is the radius of a capillary tube that would wick a given liquid at the same rate as the powder would. This straight line is in fact the solution of the Washburn equation for θ=0 and cosθ=1.

One major limitation of the wicking approach is that one cannot obtain contact angles with liquids that would produce contact angles approaching 90° or more, because in these cases the liquid cannot penetrate the porous column or layer. Another limitation lies in the fact that high viscosity contact-angle liquids such as glycerol cannot be used in wicking, owing to the enormous time span needed for each observation (cf. Eq. (3.21)). Finally, as pointed out by Yildirim [11], the thin layer wicking technique is restricted to the upper particle size of approximately 45-53 μm. When the particle size is too large, it is difficult to obtain a smooth, homogenous layer of particles on the surface of glass slide. Larger particles tend to form patches and bumps

on the glass surface and additionally the speed of the moving liquid front is to high to be accurately manually measured.

Some authors found out that the degree of scatter of data by using this technique is greater than the scatter that one encounters with direct contact-angle measurements on flat, smooth solids. The scatter is most likely due to a certain degree of variability in pore size distribution and particle packing from one slide (or column) to another. It is therefore desirable to do multiple experiments, in column as well as in thin layer wicking, to enhance the statistical significance of the average $cos\theta$ values obtained.

It should be also kept in mind that with wicking one always obtains an advancing contact angle, in the sense that for each observation the liquid is actively advancing and has not been allowed to come to rest at any point. In particular, retreating liquid/air (or liquid/vapor) contact angles cannot be observed by wicking in air or in vapor.

Finally, at least as far as thin layer wicking with rather volatile alkanes is concerned (needed for the determination of R_{eff}), it is essential to leave the thin plates in the presence of the vapor of the liquids used, for some time before the actual wicking, to obviate an undue decrease in wicking velocity due to evaporation.

With clay particles that are prone to swelling, e.g. clays from the smectite group, wicking should not be used, but swelling particles tend to form very smooth layers upon drying, so that in such cases direct contact angle measurements can be done.

3.6.2.5- Adhesive tape method

A very simple method to assess the contact angle of powdered soil samples was proposed recently by Bachmann and co-workers [82, 83]. The particles were sprinkled on double-sided adhesive tape and pressured to establish a quasi-plain surface. The

contact angles were measured immediately following the release of the pressure to avoid the interference of volatile substances from the glue of the tape. When compared with the wicking method (capillary rise) a very good agreement was obtained [83]. The main motivations of those authors that led to development of this technique was to obtain a method that was simpler and faster than the exiting procedures and that still yielded accurate and reproducible results.

It was the primary objective of the current section to study the possibility of measuring the contact angles on powdered talc samples of different fineness using the thin layer wicking method. This will allow the surface free energy parameters of solid surfaces to be calculated from the measured contact angles. Secondly, it was aimed to compare the thin layer wicking results (contact angle and surface free energies) with those obtained on polished flat talc samples, compressed pallets and loose powder deposited on adhesive tape as well.

In order to fulfill these objectives, contact angle measurements were conducted on:

i) powdered samples using the layer wicking technique;
ii) polished flat samples, compressed pellets and adhesive tape using the sessile drop technique.

The effect of grinding, and hence, the particle size, on the surface properties of talc were discussed based on the contact angle/surface free energies results.

3.7- Experimental

The run-of-mine (ROM) lump samples from the Cabeceiras deposit were received from Magnesita S.A., Brazil. They were used for contact angle measurements using the sessile drop techniques. The ground samples, from the same mine, were characterized in Chapter 1.

The contact angle measurements were conducted using apolar and polar liquids:

apolar liquids: octane, nonane, decane, undecane, diiodomethane, 1-bromonaphthalene
polar liquids: water and formamide

The former interacts with talc only through Lifshitz-van der Waals (LW) interactions, while the latter interacts with talc through both LW and hydrogen bonding (acid-base) interactions.

All of the organic liquids used in the present work were HPLC grade (>99% purity) and dried over 8 to 12 mesh 4Å (Fischer Scientific) molecular sieves before use. All experiments were conducted using deionized water[4] produced from a Barnstead E-pure water purification system. The main physical properties of the test liquids used are listed in Table 3.2.

3.7.1- Contact angle measurements: on flat surfaces

Small pieces of a representative run-of-mine talc sample from were cut to discs of about 2" diameter. Then, the discs were polished with different grades of abrasive paper, (with a grit from #60 to #1200) following a rigorous procedure developed by Drelich *et al*. [84], and then with alumina powder (Buehler 0.3 and 0.05 μm) on a rotating wheel polisher (Buehler, Ecomet III). After the final polishing, the discs were subjected to ultrasonic vibration to remove the fine abrasive particles from the surface. The samples were rinsed with ethanol and deionized water, and then dried for 3 hours at 105°C before contact angle measurements. The chemical and physical characterization of the discs are presented in Table 3.3.

[4] Electrical resistivity: 18 MΩ.cm at 25°C (min.).

Table 3.2. Physical properties of the contact angles liquids

Substance	purity	Supplier	molecular formula[1]	chemical structure[1]	Density (g/cm^3)[1]	vapor pressure[1] mm Hg @ 20°C	vapor density[1] (air = 1)	boiling point[1] (°C)	dipole moment[1] (D)	viscosity Poises, 20°C	surface tension[3], mJ/m^2 (20°C)
water	deionized	Barnsted (E-pure)	H_2O	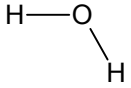	1	17.54	0.013	100	1.8546	0.01	$\gamma^{LW}= 21.8$ $\gamma^{-}= 25.5$ $\gamma^{+}= 25.5$
formamide	99.5% min	Acros	$HCONH_2$	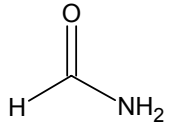	1.133	0.075	1.56	210	3.73	0.037611	$\gamma^{LW}= 39$ $\gamma^{-}= 39.6$ $\gamma^{+}= 2.28$
1-bromonaphthalene	97%	Avogrado	$C_{10}H_7Br$	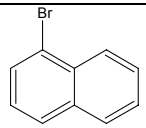	1.489	0.0062	n.d.	279-281	[1.55]	0.0489[2]	$\gamma^{LW}= 44.4$ $\gamma^{-}= 0$ $\gamma^{+}= 0$
diiodomethane	> 99%	Acros	CH_2I_2	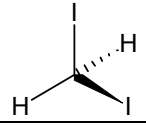	3.32	0.68	9.25	181	[1.08]	0.02821[2]	$\gamma^{LW}= 50.8$ $\gamma^{-}= 0$ $\gamma^{+}= 0$
octane	> 99%	Acros	C_8H_{18}	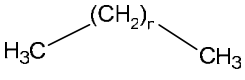 n = 6	0.708	11	3.9	126	0	0.00540[1]	$\gamma^{LW}=21.62$ $\gamma^{-}= 0$ $\gamma^{+}= 0$
Nonane	> 99%	Sigma	C_9H_{20}	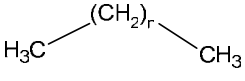 n = 7	0.718	3.22	4.41	150.8	0	0.00712[1]	$\gamma^{LW}=22.85$ $\gamma^{-}= 0$ $\gamma^{+}= 0$
Decane	> 99%	Acros	$C_{10}H_{22}$	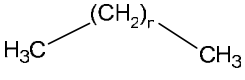 n = 8	0.73	2.7	4.9	174.1	0	0.00905[1]	$\gamma^{LW}=23.83$ $\gamma^{-}= 0$ $\gamma^{+}= 0$
Undecane	> 99%	Acros	$C_{11}H_{24}$	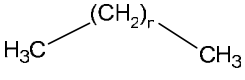 n = 9	0.74	0.28	5.4	195.9	0	0.01191[1]	$\gamma^{LW}=24.65$ $\gamma^{-}= 0$ $\gamma^{+}= 0$

Notes: 1 From ref. [85].
2 From ref. [86].
3 From ref. [16].
According to ref. [85], the dipole moment values were obtained by liquid phase measurements, which sometimes have large errors because of association effects, enclosed in brackets.

The sessile drop technique was used to measure the equilibrium contact angles of different liquids listed in Table 3.1. In this technique, a small drop of liquid (2-4 mm diameter) was placed on the surface of a polished talc plate using a microliter syringe, and the contact angle was measured through the liquid phase using an automated computer-controlled apparatus (FTA-135, First Ten Angstroms, VA). The instrument uses a CCD video camera to capture images for analysis. Contact angles are determined by means of a software (Fta32 – version 2.0) that fits a mathematical expression to the shape of the drop and then calculates the slope of the tangent to the drop at the liquid-solid-vapor (LSV) interface line [87].

Table 3.3. Chemical and physical analysis of lump talc (Cabeceiras Mine)

	% (w/w)
L.O.I.	4.83
SiO_2	63.07
TiO_2	0.01
Al_2O_3	0.36
Fe_2O_3	0.24
MnO	n.d.
CaO	n.d.
MgO	31.49
Crystalline silica	0.07
Whiteness	97.5

Note: L.O.I. – Loss on ignition.

3.7.2- On Powdered Surfaces

3.7.2.1- Thin layer wicking technique

An appropriate support for thin layer wicking consists of glass microscope slides (2.5 x 7.5 cm, or 1" x 3"). Dry talc powder (Magnesita S.A., Brazil) was dispersed in deionized water at a 4% (w/v) suspension.

Aliquots of 4.5 ml were withdrawn in a pipette and evenly distributed on clean glass microscope slides, which were kept strictly horizontal. The water was allowed to evaporate overnight at room temperature, leaving a uniform, thin deposit of the powdered mineral firmly adhering to the glass. The slides were then dried in an oven overnight at 150^{o}C and then stored in a desiccator over a desiccant, until needed for

wicking. The oven drying is necessary to eliminate any residual pore water in the powder which might interfere with the measurements by diluting some of the wicking liquids (thus changing their surface tensions and viscosities) and/or by changing the surface tension properties of the mineral surfaces.

Prior to immersion, the coated slides were kept in Petri dishes for about 72 h to allow the powder to equilibrate in the vapor of the low surface tension spreading liquids (volatile n-alkanes) [88], while no equilibration is necessary with the test liquids of high surface tension and that have contact angle higher than 10^{o} on talc surface (see Section 3.3), i.e., 1-bromonaphthalene, diiodomethane, water and formamide [70].

The thin layer wicking experiments were performed by means of an adapted horizontal chamber used for thin layer chromatography (DS-II chamber, Chromdes, Poland), following the procedure of Chibowski [89]. The only difference from the original approach was the adaptation of glass window at the bottom of the chamber that allowed the passage of light and visualization of the moving liquid front in the glass slides during the wicking process (Figure 3.6). All experiments were carried out in a close chamber. The glass slide was placed horizontally in the chamber with the talc layer facing up. Two slides were "developed" at the same time. The probe liquid was placed in one of the edges of the chamber and brought into contact with the adsorbent layer by means of another glass slide. Two scales were fixed outside the glass cover and carefully aligned with the edges of the slides to set the zero position. A cold-light lamp was placed underneath the chamber. The time required to the probe liquid to reach every 5mm interval was recorded using a stopwatch. The first 5mm were ignored. The wicking was stopped by moving back the glass slide of the liquid container. With each sample, the tests were repeated at least three times for each liquid.

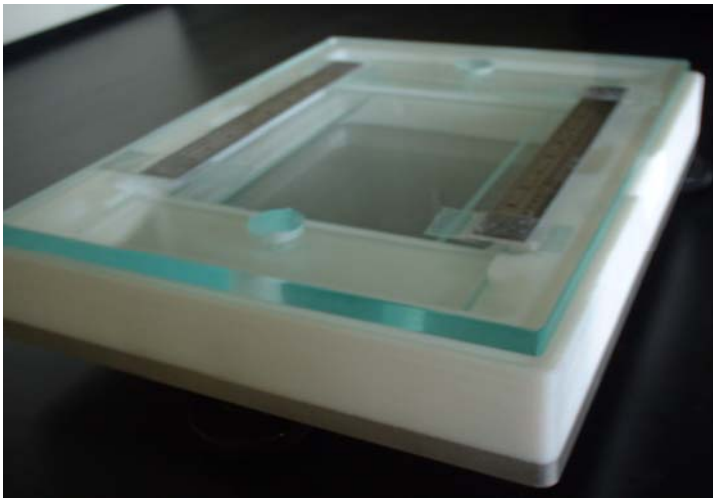

Figure 3.6 – Horizontal chamber used for the thin layer wicking experiments.

Alternatively, the thin layer wicking experiments can be performed by immersing the dried coated glass slides in the vertical position to a depth of about 5 mm in a cylindrical glass container provided with an gas-tight ground-glass stopper (weighing bottles). The vertical movement of the liquid front through the powdered layer is observed visually. The wicking is stopped (by taking the slide out of the wicking container) when the liquid had traversed a sufficient distance (usually between 1 and 5 cm). By means of small indentations applied every 5 mm to the sides of the glass slide, it is possible to make several observations of the different times, *t*, elapsed for the liquid front to reach various heights, *h*, on the thin layer column. This process yields a series of *h* and *t* values. The mentioned indentations do not interfere with the measurement [1].

Owing to various hydrodynamic disturbances occurring at the moment of immersion, it is difficult to determine the 'real' time zero (t=0) or the time when the liquid begins to wick through the powder film. It was experimentally observed [76] that especially with thin layer wicking with non-spherical particles, i.e. clay particles, one must not start counting the wicking time, *t*, from the moment of immersion. What one does instead is to determine the progression of the upward advance of the liquid front as a function of the distance *h* at various intervals of 5 mm each (beginning at 5 mm above the front of immersion) using a stopwatch.

3.7.2.2- Compressed powder

Two samples were selected for the determination of contact angle on compressed powders. Samples C and H. Sample C was chosen because it is the coarsest sample that can be used for thin layer wicking and further comparison with the compressed pellet and the adhesive tape methods. Wicking on samples A and B was tried but the liquid ascendant flow was too fast to be accurately measured. Sample H was chosen because of its maximum fineness.

To make the pellets a mass of 4.00 g of dried talc was poured into the die of highly polished stainless steel (31 mm die Spex 3623ST) and pressed using a manual hydraulic press (Carver press, model 3912). The dwell time was fixed at 1 minute but the effect of the total pressure on the contact angle was tested. Four different values were evaluated: 5,000, 10,000, 20,000 and 30,000 psi.

The sessile drop technique was used to measure the equilibrium contact angles using the same equipment as described in Section 3.8.1. The volume of the drops was about 10μL in order to minimize the gravitational effects [90].

3.7.2.3- Adhesive tape

Samples C and H were again selected for the adhesive tape method to allow the comparison between different methods. The original preparation procedure as described in Section 3.7.2.5 had to be modified due to the cohesiveness nature of talc. The sample could not be sprinkled over the tape and instead very dilute suspension of talc were prepared in water, transferred to a glass slide using a pipette and dried naturally overnight. The optimum sample concentration, 0.20% for sample C and 0.04% (w/v) for sample H, was determined by trial and error targeting, ideally, the formation of a monolayer of particles on the tape surface. Then, they were dried for 3 h at 150^{o}C and stored in a desiccator until needed. By means of a smooth double-sided copper tape (3M electrical tape), the layer of talc resting on the glass slide was peeled off from the

surface. The other side of the tape was attached to another bare glass slide. The face contained the talc was covered with a clean microscope slip and loaded with 100g weight for about 30 seconds. The cover slip was removed and slides were carefully knocked to remove surplus particles. Immediately after sample preparation the contact angles were measured. The sessile drop technique was used to measure the equilibrium contact angles using the same equipment as described in Section 3.8.1.

3.8- Results and discussion

3.8.1- Thin layer wicking

Thin layer wicking experiments yielded linear plots of h^2 vs. t, for all samples studied. In Figure 3.7, a plot of h^2 vs. t is given for alkanes (octane, nonane, decane and undecane) on sample H, while the same is given in Figure 3.8 for the other high-energy liquids used, e.g., 1-bromonaphthalene, diiodomethane, water and formamide. These 2 graphs typify the results for all analyzed samples. For both graphs the standard deviations and the correlation coefficients after linear regression are also shown. The reproducibility of the wicking experiments was very good which can be seen by the small width of the standard deviation bars in Figures 3.7 and 3.8.

The value of R_{eff} in the Washburn equation (Eq. (3.21)) for each talc powder were obtained from the plots of $2\eta h^2/t$ vs. γ_L using alkanes as the low-energy wetting liquids. A sample plot for determining R_{eff} using alkanes in the thin layer wicking experiments is given in Figure 3.9 for sample C. As shown, the plot of $2\eta h^2/t$ vs. γ_L yields a straight line passing through origin whose slope is R_{eff} [76].

The values of average particle size (d_{50}) and mean capilary radius (R_{eff}) for various talc powders are given in Table 3.4 and plotted in Figure 3.10. As shown, the value of R_{eff} determined from thin layer wicking measurements is mainly dependent on the particle size, but other variables such as the origin of talc ore, aspect ratio, surface treatment etc. may also influence the magnitude of R_{eff}. Generally, as the particle size

is finer, the value of R_{eff} becomes smaller since the packing efficiency is increased, i.e., the radii of the capillary bundle tends to be smaller. For example, the value of R_{eff} is 0.456 μm for sample B which has a d_{50} of 7.5 μm, whereas it is 0.046 μm for sample H whose mean particle size is 0.39 μm.

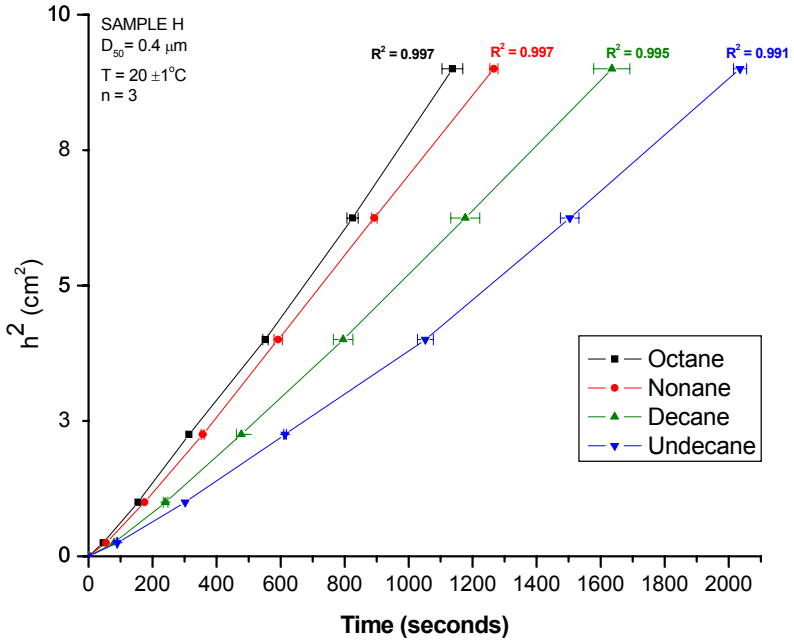

Figure 3.7 – Squared distance vs. penetration time for for the wicking of n-alkanes in talc layer (sample H) at 20±2°C.

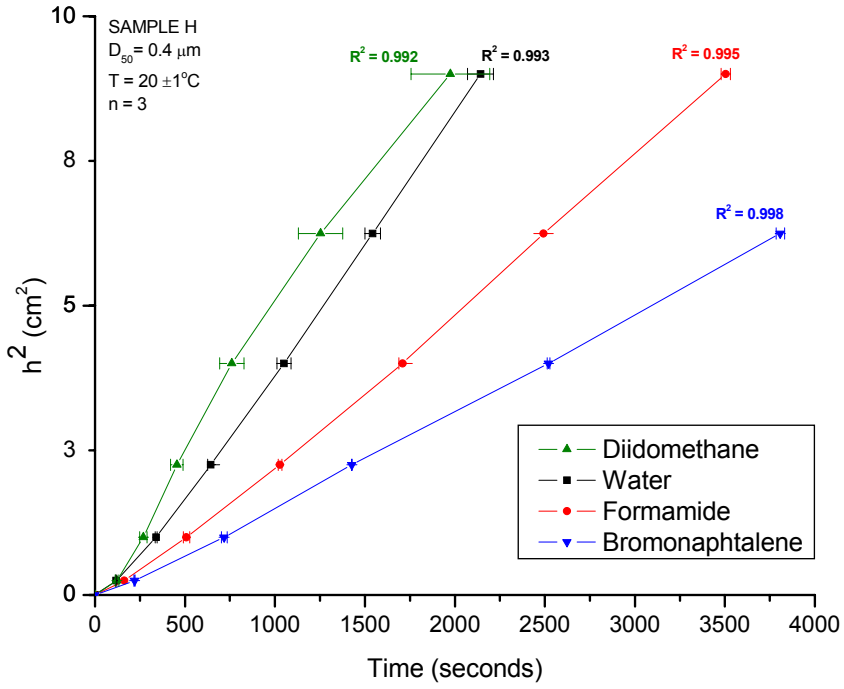

Figure 3.8 – Squared distance vs. penetration time for the wicking of high-energy liquids in talc layer (sample H) at 20°C.

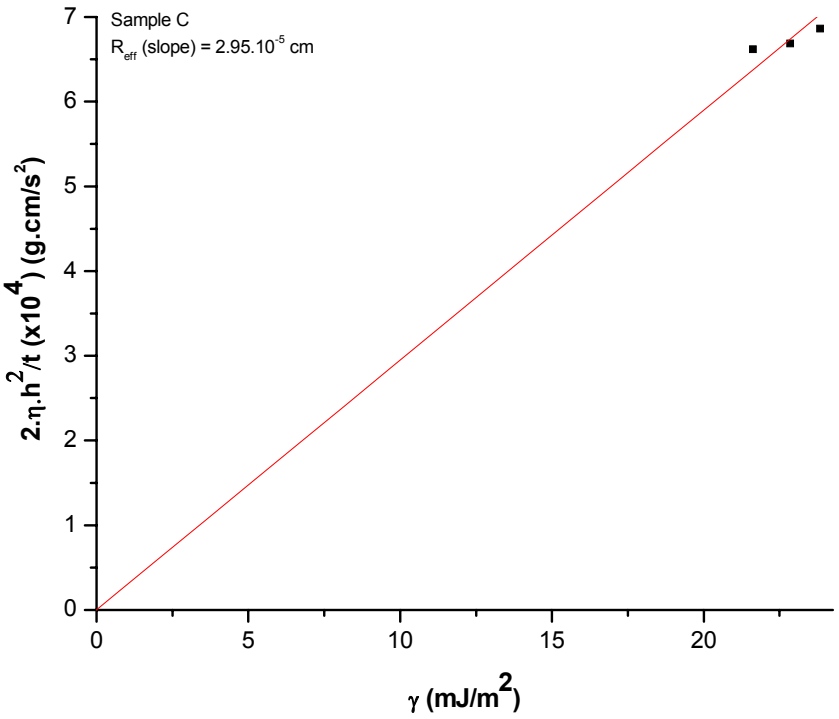

Figure 3.9 – Plot of Wicking coefficient vs. liquid surface tension for the determination of R_{eff} (sample C) at 20°C.

Table 3.4. Average capillary radius (R_{eff}) determined by thin layer wicking on various talc powders (at 20±2 °C)

Talc sample	Average particle size (μm)	R_{eff} (μm)
B	7.5	0.456
C	4.49	0.295
D	1.53	0.129
E	1.35	0.076
F	1.15	0.091
G	0.49	0.055
H	0.39	0.046

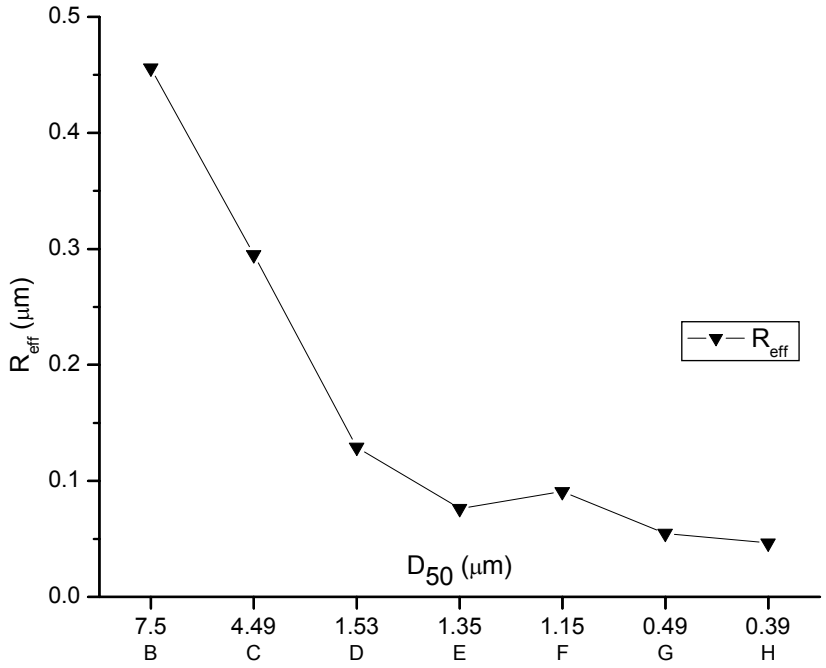

Figure 3.10 - Plot of effective capillary radius (R_{eff}) vs. average particle size (D_{50}).

The advancing contact angles of various liquids on the powdered talc samples obtained from thin layer wicking measurements are given in Table 3.5. As shown, the values of advancing water contact angles for various talc powders were in the range of

76 and 86°. The data suggest that the most hydrophobic powders are samples B and D, with sample H being the most hydrophilic.

Table 3.5. Contact angles θ (deg) of various liquids on powdered talc samples measured using thin layer wicking technique (at 20±2 °C)

Sample	Average particle size (μm)	W	FO	1-Br	DI
B	7.5	85.87	51.70	36.11	55.05
C	4.49	83.48	60.15	55.05	57.76
D	1.53	85.73	63.85	44.81	54.55
E	1.35	80.92	60.96	36.47	29.82
F	1.15	82.96	52.75	38.89	45.14
G	0.49	78.30	50.95	40.15	43.60
H	0.39	76.07	45.61	43.35	50.58

W=Water, FO=Formamide, 1-Br=1-Bromonapthalene, DI=Diiodomethane

The equilibrium contact angles measured using the sessile drop technique on the flat surfaces of Cabeceiras Mine samples are given in Table 3.6. The highest values were obtained with water. By comparing Tables 3.5 and 3.6 one may observe that the contact angles measured thin layer wicking techniques on the powdered surfaces are invariably higher than those measured by using sessile drop on the flat surfaces. For example, the advancing water contact angle was 60° on the flat Cabeceiras talc surface, whereas it became in average higher than 80° for powdered samples resulting from the same ore. The water contact angle on flat talc surface reported here showed a very good agreement with data from literature. Doulliard *et al*. [91] found also 60° and Schrader and Yariv [68] found 61°.

A reasonable explanation for obtaining higher advancing water contact angles on the ground samples would be that the surface properties of talc are changed significantly because of mechanical grinding. More hydrophobic basal plane surfaces were exposed upon comminution; as a result, water contact angle is increased. The increase in the value of contact angles for the other test liquids can also be explained in

the same sense, e.g. the surface free energy of talc was reduced after the grinding due to the creation of more basal surfaces. Additionally, as pointed out by Yariv [69], the contact angle on a flat surface represents an average value of randomly oriented crystals while values in the order of 80^{o} seems to be most representative of that of the (001) hydrophobic basal plane.

A very low value of the contact angle for 1-bromonaphtalene was obtained for the flat surface, but it was not observed spreading: the drops were very flat, but stayed on the surface of talc. This means that the apolar component of the surface free energy of talc (γ_S^{LW}) has to be lower than 44.4 mJ/m^2, which is the apolar component of 1-bromonaphthalne, otherwise the liquid would completely spread over the surface. Indeed, for all the wicking experiments involving all samples the highest γ_S^{LW} obtained was for sample B (γ_S^{LW} =36.28 mJ/m^2).

In the present work, the measured values of advancing water contact angle on various powdered talc samples (thin layer wicking) were in the range of 76 to 86 (see Tables 3.5). Wu and co-workers [70], using thin layer wicking for talc, reported 79.3^{o}. Yariv, using a method similar to the adhesive tape [69], reported an advancing water contact angle for talc of 83^{o}. Fowkes and Harkins [67] reported values of about 84^{o} and 88^{o} in two different flat talc samples that were carefully cleaved along the 001 plane. Hence, the contact angle data reported here is in agreement with what has been published in the literature. Nonetheless, it can be expected that the origin of talc ore, surface preparation techniques, processing, particle size etc. may affect the surface hydrophobicity, and thus the value of the contact angle.

Finally, the results of the contact angle with water (Table 3.5) also suggest that after a given fineness the contact angle with water starts to decrease, i. e., which probably means that more edge surfaces are being created by breaking the hydrophobic basal surfaces. The evidence would appear to suggest that there is a limit in terms of hydrophobicity that can be achieved using the grinding technology employed here.

Table 3.6. Contact angle and surface free energy measurements for lump talc at 25°C

	Contact angle (°)					Surface free energy components (mJ/m^2)					
	Water	Formamide	Diiodomethane	1-bromonaphthalne	heptane	γ_S^{LW}	$\gamma_S^{\ominus}$	$\gamma_S^{\oplus}$	γ_S^{AB}	γ_S^{Total}	Polarity (%)
Lump (Magnesita)	60.0	41.0	45.0	< 1	spreads	37.01	17.04	1.12	8.74	45.75	19.1
Lump (Luzenac)*	60.0	42.0	38.0	< 1	n.d.	40.60	17.84	0.49	5.88	46.49	12.7

Note: * Contact angle values obtained from ref. [91].

3.8.2- Surface free energies of talc

The values of contact angles given in Table 3.6 for the sessile drop technique on flat talc surface were used to calculate the Lifshitz-van der Waals (γ_S^{LW}), Lewis electron donor ($\gamma_S^{\ominus}$) and electron acceptor ($\gamma_S^{\oplus}$) components of the surface free energies on the Cabeceiras talc samples using Eq. (3.9). As discussed before, the calculation requires a set of three contact angles for three different liquids, along with their surface tension components. The values of γ_L^{LW}, $\gamma_L^{\ominus}$, and $\gamma_L^{\oplus}$ for liquids were taken from the literature (see Table 3.1). Diiodomethane-water-formamide were used to calculate the values of γ_S^{LW}, $\gamma_S^{\ominus}$ and electron acceptor $\gamma_S^{\oplus}$ components of the surface free energy of talc samples. The results are shown in Table 3.6. Also shown in this table are the values of γ_S^{AB} and γ_S^{Total} calculated using Eqs. (2.38) and (3.11), respectively. The polarity (%) is defined as:

$$\text{polarity}(\%) = \frac{\gamma_S^{AB}}{\gamma_S^{Total}}.100 \tag{3.22}$$

Similar calculations were also made from the contact angle data reported for the thin layer wicking technique. For a given talc surface, the advancing contact angles (θ_a) measured using two test liquids triplets; i.e., water/formamide/diiodomethane and water/formamide/1-bromonaphthalene were used for calculating the surface free energy components of talc surfaces. The advancing contact angle is generally considered to be the intrinsic contact angle of the surface with microscopic heterogeneity [53-55]. Based on the values of θ_a obtained for these liquids, Eq. (3.9) was solved simultaneously to obtain the values of the relevant surface free energy components.

Table 3.7 gives the values of surface free energy parameters γ_S^{LW}, $\gamma_S^{\ominus}$, $\gamma_S^{\oplus}$ and γ_S^{AB} obtained from the thin layer wicking measurements for various powdered talc surfaces. It can be seen, by comparing Tables 3.6 and 3.7, that the surface free energy components of ground talc particles are different from those of original flat samples. As

mentioned earlier, mechanical grinding causes considerable changes in both the Lifshitz-van der Waals component and the Lewis acid-base parameters. For example, the γ_S^{LW} for the lump talc decreased from 37.0 mJ/m^2 on the flat surface to 31.7 mJ/m^2 on the powdered surface that has an average particle size of 4.5 μm (sample C). Also shown in Table 3.7, the value of $\gamma_S^{\ominus}$ somehow changed from the original flat surface to the ground surface, while the $\gamma_S^{\oplus}$ remained practically unchanged. The γ_S^{AB} also decreased when the particles were pulverized. For example, the γ_S^{AB} was 8.74 mJ/m^2 on the flat Cabeceiras talc surface, while it decreased to 3.4 mJ/m^2 (average) on the ground samples. The value of γ_S^{Total} on the Cabeceiras talc surfaces also decreased when the samples were ground. The decrease in the value of γ_S^{Total} is achieved due to the decrease in the values of both γ_S^{LW} and γ_S^{AB}.

Wu *et al*. [70] studied the effect of comminution on the surface properties of talc and found that the surface of minerals become more hydrophobic upon grinding. The evidence presented here would appear to suggest that the main reason for the decrease in the values of both γ_S^{LW} and γ_S^{AB} is the creation of more hydrophobic basal plane surfaces on the ground samples.

Considering the crystal structure of talc, the talc particles have the shape of platelets due to the layer structure of the mineral. The atoms within the layers are held together by ionic bonds, while the oxygen-oxygen interlayer atoms (linked together by siloxane bonds) by weak van der Waals forces [7-9]. As a result, easy breakage takes place along the layers that are termed as the “basal planes”. Since the basal planes are composed predominantly of Lifshitz-van der Waals component of surface free energy, it can be predicted that the total surface free energy (γ_S^{Total}) at the basal plane surface should be lower than the total surface free energy at the edge surface. Apolar surfaces, e.g. Teflon, are known to possess only the γ_S^{LW}; therefore, their total surface free energy

is usually lower than the polar surfaces that have both γ_S^{LW} and γ_S^{AB} surface free energy components (e.g. metals, hydrophilic minerals).

The surface free energy parameters γ_S^{LW}, $\gamma_S^{\ominus}$, $\gamma_S^{\oplus}$ and γ_S^{AB} obtained from the thin layer wicking were plotted as a function of average particle sizes (D_{50}) in Figure 3.11. The values of $\gamma_S^{\ominus}$ increase with decreasing particle size down to the average particle size of ≅ 1.5 μm after which it starts to decrease again. The opposite is true for the $\gamma_S^{\oplus}$ parameter, i.e., it first decreases down to the particle size of ≅ 1.5 μm and then it increases. The values for γ_S^{AB} are nearly the same over down to the particle size of ≅ 1.5 μm due to the balance in the $\gamma_S^{\ominus}/\gamma_S^{\oplus}$ parameters. However, there is a clear trend of increasing in the value of the γ_S^{AB} for the finer samples (F, G and H) and, consequently, the total polarity also increases significantly. Also shown, the decrease in the value of γ_S^{Total} is primarily attributed to the decrease in the value of γ_S^{LW} down to the limit size of ≅ 1.5 μm. After that the γ_S^{Total} shows a trend to increase as a reflex of primarily the increase of the γ_S^{AB} component.

Table 3.7. Surface free energy and its components of powdered talc samples obtained from thin layer wicking measurements

Talc sample	Average particle size D_{50}, (μm)	Surface Free Energy, mJ/m^2					
		γ_S^{LW}	$\gamma_S^{\ominus}$	$\gamma_S^{\oplus}$	γ_S^{AB}	γ_S^{Total}	Polarity (%)
B	7.5	36.28	0.78	1.63	2.25	38.53	5.84
C	4.49	31.73	3.93	0.70	3.32	35.05	9.47
D	1.53	32.44	3.85	0.27	2.03	34.47	5.89
E	1.35	36.13	6.30	0.08	1.40	37.53	3.72
F	1.15	35.10	2.07	1.38	3.38	38.48	8.78
G	0.49	34.55	4.19	1.41	4.86	39.42	12.33
H	0.39	33.11	3.90	2.72	6.51	39.62	16.43

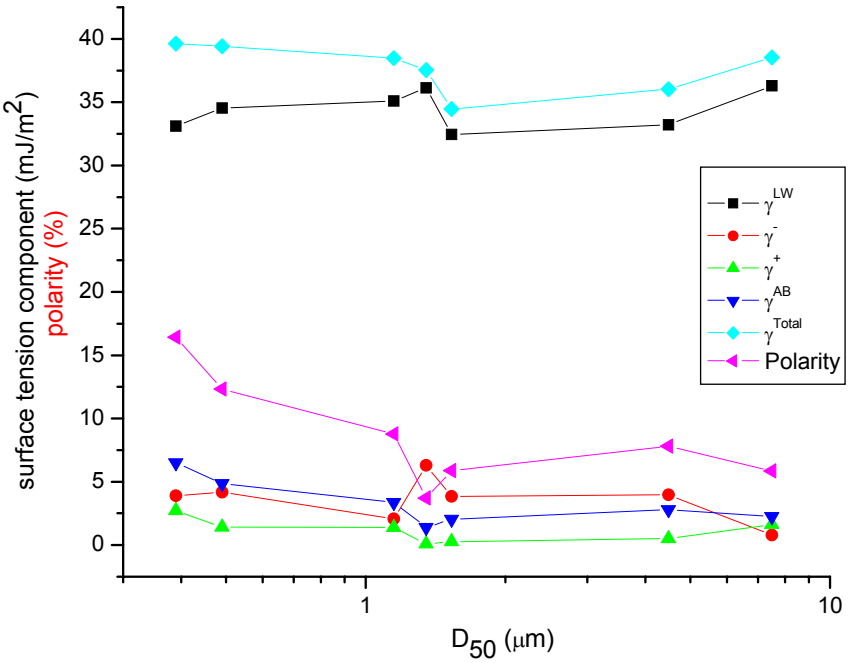

Figure 3.11 – Surface free energy components (mJ/m^2) and polarity (%) vs. average particle size (D_{50}).

The results presented throughout this work have consistently demonstrated that the surface of talc is predominantly basic, but there are also few acidic sites. As shown in Figure 1.9, the basal planes of talc are made up of O atoms that are linked together by Si-0-Si bonds, while the edges are composed of Mg-OH, Si-OH and the other substituted cations, e.g. Al^{3+}, Fe^{2+}, as discussed in Chapter 1. Among those Mg-OH is slightly basic, while the Si-OH group on the edge surfaces are acidic in character. Ideally, the ratio of Si-OH/Mg-OH in a single layer is 2:1 which theoretically would result in a predominantly acidic character at the edges. The ditrigonal cavities of the basal planes, in turn, have a weak basic character due to the six sets of lone-pair electron orbitals on the oxygens atoms (see Section 1.5.1). Yildirim have indeed confirmed the monopolar basic character of the basal planes and the monopolar acidic character of the edges using an original methodology that combines flow microcalorimetry and thin layer wicking [11]. Similar results were found in this investigation and are described in Chapter 5.

In the light of the these statements, it becomes clear that an increase in the percentage of basal planes would result in the increase of the $\gamma_S^{\ominus}$ and concomitant decrease of $\gamma_S^{\oplus}$. This was indeed what happened down the particle size of about ≅ 1.5 μm. On the contrary, an increase in the egde surfaces would give a higher value of $\gamma_S^{\oplus}$ and lower $\gamma_S^{\ominus}$, which was observed for particle sizes finer than 1.5 μm. Additionally, for particles finer than 1.5 μm a clear increase of polarity (hydrophilicity) was noted. The increase in the polarity is in good agreement with the determined values for water contact angle, which decreased.

Again, there seems to be a limit in terms of delamination that can be achieved using the grinding technology used here after which the lamellae start to fracture across the basal planes generating more hydrophilic edge surfaces.

Comminution is one important physical treatment to which powders are often subjected to. There are reports in the literature which show that the choice of milling technique can be important in controlling the ultimate surface properties of a powder. Hansford *et al*. [92] reported that the contact angles, varied for griseofulvin[5] depending upon the milling process used. Buckton *et al.* [93] studied powder/water interactions by vapor adsorption using the vacuum microbalance (to obtain ΔG_{ads}) and the microcalorimetric (to obtain ΔH_{ads}) techniques [94]. Six different samples of aspirin were prepared by use of the six different grinding technologies. An important conclusion from that work was that the milling process alters the energetics of the powder surface such that a powder milled by one process may be satisfactory for a given application, but the same powder milled by a different process may not be.

Considering that the surface free energy of a surface plays a major role in controlling the behavior of any system, it is evident that the choice of size reduction process can be a crucial factor in controlling product performance.

[5] Griseofulvin is a powder of pharmaceutical use.

3.8.3- Comparison of different methods

Table 3.7 and 3.8 contain the results for contact angle measurements using three different methods for samples C and H respectively, which are plotted in Figures 3.12 and 3.13 for sample C and Figures 3.14 and 3.15 for sample H. The tables compare the three different methods for powders tested in this investigation, namely thin layer wicking, compressed pellet and adhesive tape.

Prior to contact angle measurements using the compressed pellets, shown below, a separate investigation was conducted to determine the influence the pressure on the contact angle and liquid adsorption time. The results are plotted in Figures 3.12 and 3.13 below.

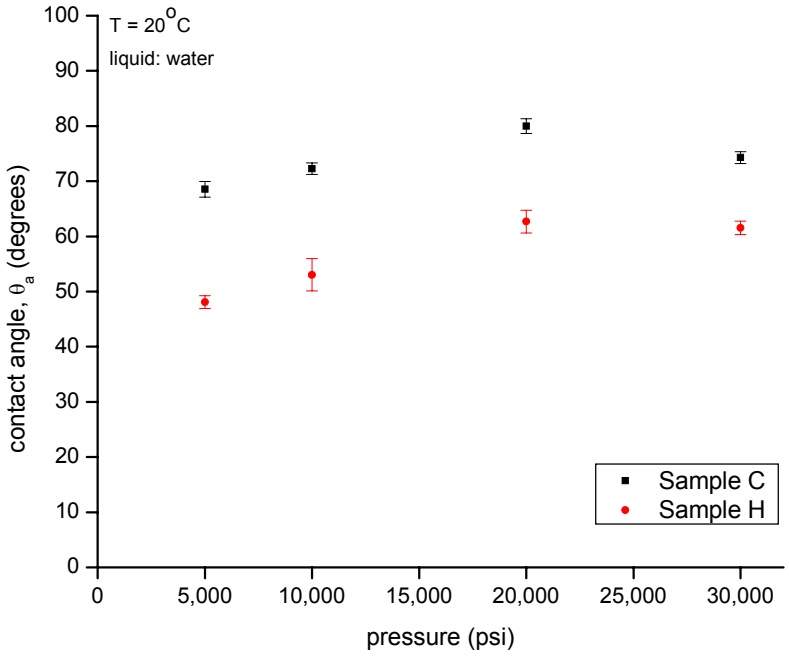

Figure 3.12. Contac angle as a function of compression force for talc.

The change in contact angle with the pressure has been investigated by some authors. It is believed that the effect of the pressure is unpredictable and depends of the material considered [95, 96]. For the case of talc, as shown in Figure 3.12, the contact angle for both samples increased with increasing the pressure and then it either leveled off or started to decrease. This could be due to the increase in the orientation of the talc

lamellae at the surface of the pellets, by increasing the compacting pressure, with the 001 planes being oriented more parallel to the surface. After a maximum pressure, the damage to the structure of the mineral could be responsible for the decrease in contact angle. Following other works published on literature [97], the 20,000 psi pressure was selected for contact angle determination with water, formamide and diiodomethane using the technique described in Section 3.8.1.

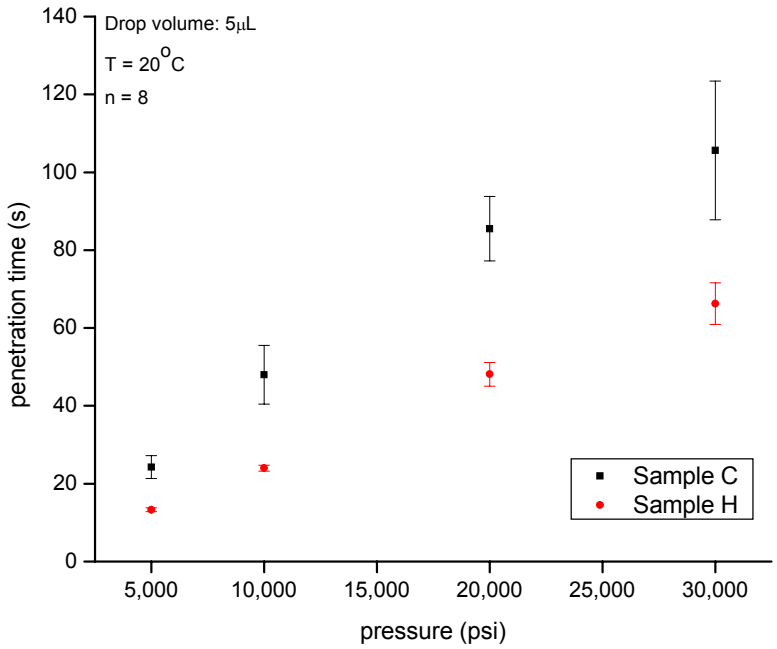

Figure 3.13. Liquid penetration time as a function of compression force for talc.

Figure above suggests that the time need for a 5μL water droplet to completely disappear from the talc surface is directly proportional to the applied pressure for both samples. As the applied pressure increases the surface roughness tend to decrease as well as the number of capillaries, causing the increase in the penetration time. Similar results have been obtained by other authors [98].

Adsorption process at the surface is indeed a complicating factor when measuring sessile drop contact angle on porous materials due to the disappearance of the drop and thus causing an underestimation of contact angle [99]. The results strengthen the need of measuring the contact angle as close as possible to the exact time the drop first

contacts the surface, as recommended by Stamm and co-workers [100]. The penetration time for sample H was faster probably due to the fact it is a more hydrophilic material and due to the formation of narrower capillaries.

As shown in Figure 3.14, it is interesting to note that for the coarse sample C (D_{50} = 4.49 μm) the contact angle with water had a very small variation for the three methods tested ($\Delta\theta$ = 3.5°). However, the contact angle for diiodomethane and formamide were significantly lower than the thin layer wicking but very similar to each other in the case of adhesive tape and compressed pellet. Consequently, the value of γ_S^{Total} increased, compared to thin layer wicking, due to mainly an increase in γ_S^{LW}, which is directly related to the contact angle with diiodomethane. The γ_S^{AB} and polarity remained practically unaltered (Figure 3.15).

For the finest sample H (D_{50} = 0.39 μm) there was no significant difference in contact angle values and thus in the surface free energy components between thin layer wicking and the adhesive tape method. For the compressed pellet all the contact angles with the 3 liquids were significantly lower than the other 2 methods. As a result, the γ_S^{Total} was higher mainly due to an increase in γ_S^{LW}. The lower values of contact angle related to compressed pellet method can be associated to the problems caused by compression.

Table 3.8. Sample C

	Contact angle (°)			Surface free energy components (mJ/m^2)					
	water	formamide	Diiodo	γ_S^{LW}	$\gamma_S^{\ominus}$	$\gamma_S^{\oplus}$	γ_S^{AB}	γ_S^{Total}	Polarity (%)
thin layer wicking	83.5	60.2	57.8	29.86	3.87	1.01	3.96	33.83	11.71
compressed pellet	80.0	45.0	42.0	38.59	1.78	1.91	3.69	42.28	8.72
adhesive tape	81.2	45.0	47.0	35.93	1.25	2.72	3.69	39.62	9.32

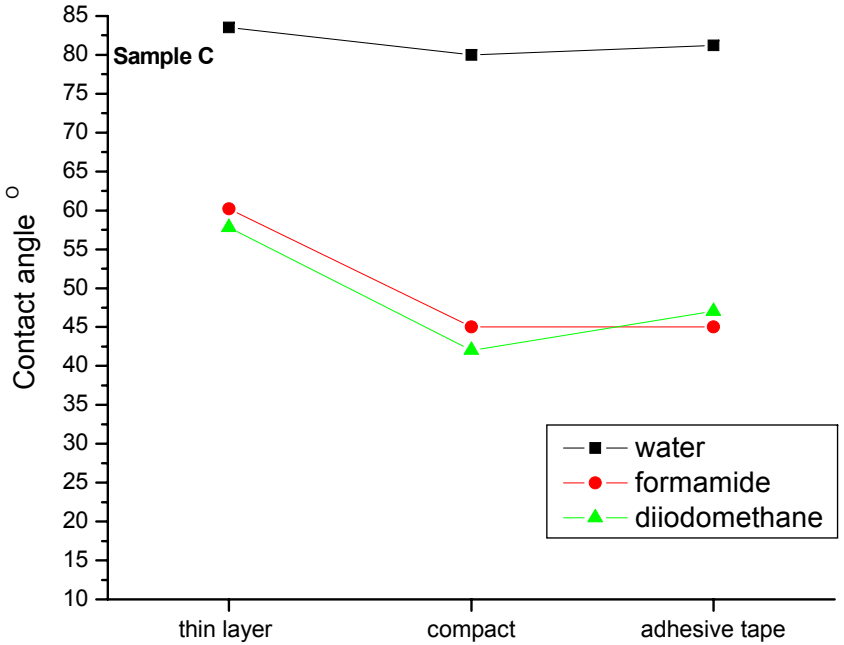

Figure 3.14. Effect of the contact angle measurement method on the value contact angle for sample C.

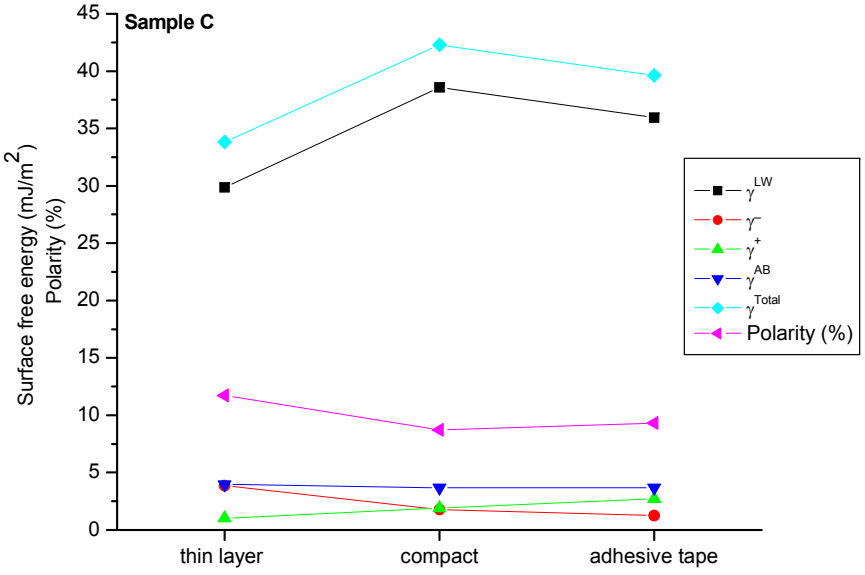

Figure 3.15. Effect of the contact angle measurement method on the value of surface free energy components for sample C.

Table 3.9. Sample H

	Contact angle (°)			Surface free energy components (mJ/m^2)					
	Water	formamide	diiodo	γ_S^{LW}	$\gamma_S^{\ominus}$	$\gamma_S^{\oplus}$	γ_S^{AB}	γ_S^{Total}	Polarity (%)
thin layer wicking	76.1	45.6	50.6	33.95	3.92	2.48	6.24	40.19	15.52
compressed pellet	65.0	29.0	32.0	43.37	7.36	2.11	7.88	51.26	15.38
adhesive tape	79.0	52.0	48.0	35.38	4.11	1.12	4.28	39.67	10.80

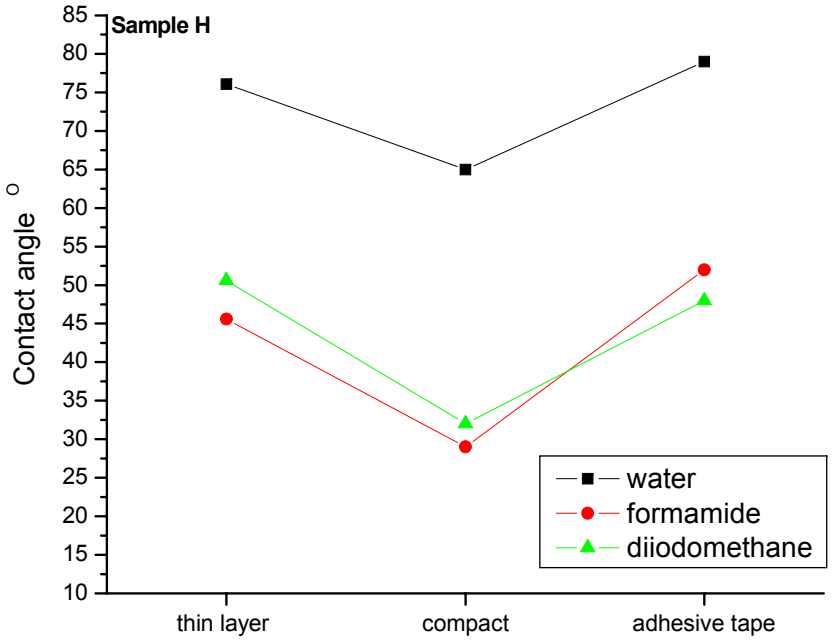

Figure 3.16. Effect of the contact angle measurement method on the value of contact angle for sample H.

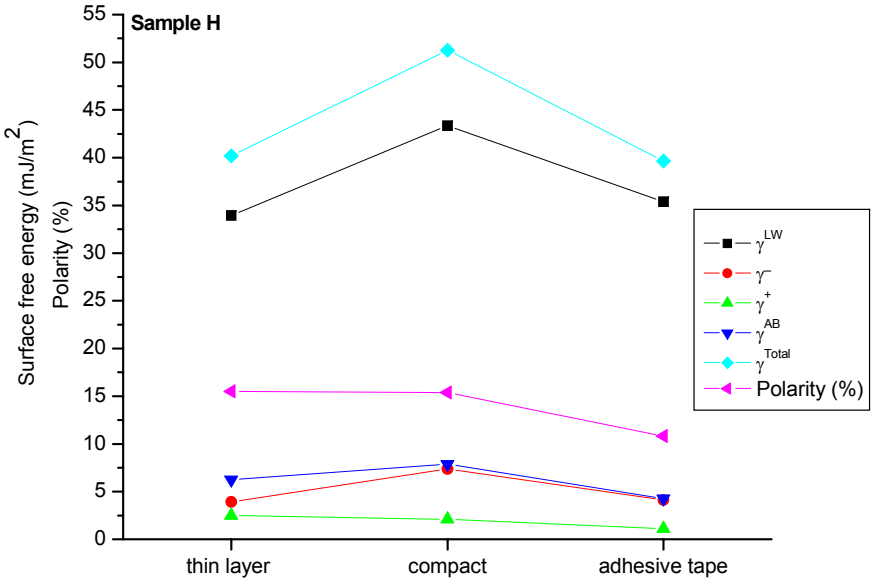

Figure 3.17. Effect of the contact angle measurement method on the value of surface free energy components for sample H.

3.9- Conclusions

Contact angle measurements were conducted on flat and powdered surfaces to determine the surface free energy components (γ_S^{LW}, $\gamma_S^{\ominus}$, $\gamma_S^{\oplus}$ and γ_S^{AB}) of talc samples using the van Oss, Chaudhury and Good (OCG) thermodynamic approach for solids. The results showed that there is a relationship between particle size and the measured contact angles. As the particle size decreases water contact angle increases up to a limit, which can be attributed due to the fact that more apolar basal plane surfaces are created. However, decreasing the particle size more than the approximate size limit of D_{50}=1.5μm (based on sedimentation) cannot be accomplished without significant fracture of the lamellae which generates more edge surfaces and increases the overall hydrophilicity of talc, decreasing the water contact angle.

The results also showed that the surface of talc contains both basic and acidic sites. However, the number of basic sites is larger than the number of acidic sites as defined from the application of OCG equation, i.e., the higher magnitude of the $\gamma_S^{\ominus}$ parameter.

As a general trend, the γ_S^{LW} and γ_S^{AB} components of surface free energy decrease with decreasing particle size, and so does the value of γ_S^{Total}. A linkage between particle hydrophobicity and surface free energy components was established. The more the hydrophobic surface is the lower the γ_S^{Total} is. However, after the limiting particle size, the value of γ_S^{Total} increases again due to possibly the creation of more edge surfaces and to the increase of the polarity.

A very good agreement between the surface free energy calculations using different contact angle determination methods has been demonstrated, especially for the coarse sample C. For the fine sample H, there was no

significant difference between thin layer wicking and the adhesive tape method. The compact pellet, however, gave a significant higher value for γ_S^{LW} and consequently for γ_S^{Total}. It is possible that more tests need to be done to draw more general conclusion about the comparison between different methods.

As pointed out by Buckton, all contact angle approaches for powdered samples have its disadvantages for some reason and to some extent [95, 99, 101, 102]. Although it is time consuming and has some others limitations (see Section 3.6.2.4.2), the thin layer wicking technique was able to reasonably detect the changes in the surface free energy of talc due to the different grinding systems, i.e., due to different ratio basal/edge surfaces.

The adhesive tape turned out to be a method very simple to perform that surprisingly did not differ very much from the results obtained by thin layer wicking. Another advantage of this method is the fact that it is not limited for contact angles below 90°, as is the case of the former. Nonetheless, there are just a few data on literature mentioning the adhesive tape method and further investigation has to be done.

The compact pellet, which is also not limited for contact angles below 90°, was very simple to be executed. However, the apolar surface free energy components tended to be higher when compared to the other methods and, as a result, so does the value of γ_S^{Total}.

3.10- References

1. van Oss, C.J. and R.F. Giese, *Colloid and surface properties of clay and related minerals*. 2002, New York: Marcel Dekker.

2. Norris, J.G., *Surface free energy of smectite clay minerals*, in *SUNY*. 1993: Buffalo.

3. Lyklema, J., *Fundamentals of Interface and Colloid Science*. Vol. III: Liquid-Fluid Interfaces. 1991: Academic Press.

4. Good, R.J., *Contact angles and the surface free energy of solids*, in *Surface and Colloid Science*. 1979, Plenum Press.

5. Brady, P.V., *Physical and chemistry of mineral surfaces*. !996, New York: CRC Press.

6. Vaughan, D.J. and R.A.D. Pattrick, *The Mineralogical Society Series - Mineral Surfaces*. 1995, Great Britain: Chapman&Hall.

7. Etzler, F.M., *Characterization of surface free energies and surface chemistry of solids*, in *Contact angle, Wettability and Adhesion*, K.L. Mittal, Editor. 2003, VSP: The Netherlands. p. 219-264.

8. Young, T., *An essay on the cohesion of fluids.* Philosophical Transactions of the Royal Society of London, 1805. **95**: p. 65-87.

9. Lam, C.N.C.*, et al.*, *Measuring contact angle*, in *Handbook of applied surface and colloid chemistry*, K. Holmberg, D.O. Shah, and M.J. Schwuger, Editors. 2002, John Wiley & Sons: New York.

10. Bangham, D.H. and R.I. Razouk, *Adsorption and wettability of solid surfaces.* Transactions of the Faraday Society, 1937. **33**: p. 1459-1463.

11. Yildirim, I., *Surface Free Energy Characterization of Powders*. 2001, Virginia Tech.

12. Chaudhury, M.K., *Short range and long range forces in colloidal and macroscopic systems*. 1984, SUNNY: Buffalo.

13. Good, R.J., *Contact angle, wetting, and adhesion: a critical review.* Journal of Adhesion Science and Technology, 1992. **6**(12): p. 1269-1302.

14. Wu, S., *Interfacial Thermodynamics*, in *Polymer Interface and Adhesion*. 1982, Marcel Dekker: New York.

15. Fowkes, F.M.*, et al.*, *Contact angles and the equilibrium spreading pressures of liquids on hydrophobic solids.* Journal of Colloid and Interface Science, 1980. **78**(1): p. 200-206.

16. van Oss, C.J., *Interfacial Forces in Aqueous Media*. 1994, New York: Marcel Dekker.

17. van Oss, C.J.*, et al.*, *On the degree to which the contact angle is affected by the adsorption onto a solid surface of vapor molecules originating from the liquid drop.* Journal of Dispersion Science and Technology, 1998. **19**(6-7): p. 1221-1236.

18. Good, R.J.*, et al.*, *Theory of the acid-base hydrogen bonding interactions, contact angles, and the hysteresis of wetting: application to coal and graphite surfaces.* Journal of Adhesion Science and Technology, 1990. **4**(8): p. 607-617.

19. Packham, D.E., *Work of adhesion: contact angles and contact mechanics.* International Journal of Adhesion and Adhesives, 1996. **16**: p. 121-128.

20. van Oss, C.J.*, et al.*, *Monopolar surfaces.* Advances in Colloid and Interface Science, 1987. **28**: p. 35-64.

21. van Oss, C.J.*, et al.*, *Interfacial Lifshitz-van der Waals and polar interactions in macroscopic systems.* Chemical Reviews., 1988. **88**: p. 927-941.

22. Wennerstrom, H. and D.F. Evans, *The Colloidal Domain*. 1999: Willey-VCH.

23. de Gennes, P.G., *Dynamics of Wetting*, in *Liquids at Interfaces*. 1990, North Holland: Amsterdam. p. 273-291.

24. Rowe, R.C., *Binder-substrate interactions in granulation: a theoretical approach based on surface free energy and polarity.* International Journal of Pharmaceutics, 1989. **52**(2): p. 149-154.

25. Buckton, G., *The estimation and application of surface energy data for powdered systems.* Drug Development and Industrial Pharmacy, 1992. **18**(11-12): p. 1149-1167.

26. Lyklema, J., *Fundamentals of Interface and Colloid Science*. Vol. volume I: Fundamentals. 1991: Academic Press.

27. Onda, T.*, et al.*, *Super-water-repellent fractal surfaces.* Langmuir, 1996. **12**(9): p. 2125-2127.

28. Johnson, R.E.J. and R.H. Dettre, *Contact angle hysteresis III. Study of an idealized heterogeneous surface.* Journal of Physical Chemistry, 1964. **68**: p. 1744-1750.

29. Dettre, R.H. and R.E.J. Johnson, *Contact angle hysteresis IV. Contact angle measurements on heterogeneous surfaces.* Journal of Physical Chemistry, 1965. **69**: p. 1507-1515.

30. Adamson, A.W., *Physical Chemistry of Surfaces*. 1990, New York: Wiley-Interscience.

31. Kwok, D.Y.*, et al.*, *Measuring and interpreting contact angles: a complex issue.* Colloids and Surfaces A: Physicochemical and Engineering Aspects, 1998. **142**(2-3): p. 219-235.

32. Kwok, D.Y.*, et al.*, *Low-Rate dynamic contact angles on poly(methyl methacrylate) and the determination of solid surface tensions.* Journal of Colloid and Interface Science, 1998. **206**: p. 44-51.

33. Neumann, A.W. and R.J. Good, *Techniques of measuring contact angles*, in *Surface and Colloid Science*, R.J. Good and R.R. Stromberg, Editors. 1979, Plenum Press: New York. p. 31-91.

34. Li, D.*, et al.*, *Contact angle measurement by axisymmetric drop shape analysis (ADSA).* Advances in Colloid and Interface Science, 1992. **39**: p. 347-382.

35. Cheng, P.*, et al.*, *Automation of axisymmetric drop shape analysis for measurements of interfacial tensions and contact angles.* Colloids and Surfaces, 1990. **43**(2): p. 151-167.

36. Rio, O.I.d. and A.W. Neumann, *Axisymmetric Drop Shape Analysis: Computational Methods for the Measurement of Interfacial Properties from the Shape and Dimensions of Pendant and Sessile Drops.* Journal of Colloid and Interface Science, 1997. **196**(2): p. 136-147.

37. Spelt, J.K.*, et al.*, *Sessile-drop contact angle measurements using axisymmetric drop shape analysis.* Colloids and Surfaces, 1987. **24**(2-3): p. 127-137.

38. Neumann, A.W. and W. Tanner, *The temperature dependence of contact angles - polytetrafluoroethylene / n-decane.* Journal of Colloid and Interface Science, 1970. **34**(1): p. 1-8.

39. Gu, Y., *Contact angle measurement techniques for determination of wettability*, in *Encyclopedia of Colloid and Surface Science*. 2002. p. 1213-1227.

40. Masliyah, J.H. and Z. Xu, *Contact angle measurements on oxide and relataed surfaces*, in *Encyclopedia of Colloid and Surface Science*. 2002. p. 1228-1241.

41. Kwok, D.Y., *et al.*, *Capillary rise at a vertical plate as a contact angle technique*, in *Applied surface thermodynamics*, A.W. Neumann and J.K. Spelt, Editors. 1996, Marcel Dekker: New York. p. 413-440.

42. Neumann, A.W. and C.J. Budziak, *Automation of the capillary rise technique for measuring contact angles.* Colloids and Surfaces, 1990. **43**: p. 279.-293.

43. Neumann, A.W., *Contact angles and their temperature dependence: thermodynamic status, measurement, interpretation and application.* Advances in Colloid and Interface Science, 1974. **4**: p. 105-191.

44. Buckton, G., *Surface characterization: understanding sources of variability in the production and use of pharmaceuticals.* Journal of Pharmacy and Pharmacology, 1995. **47**: p. 265-275.

45. Buckton, G. and J.M. Newton, *Assessment of the wettability of powders by use of compressed powder discs.* Powder Technology, 1986. **46**(2-3): p. 201-208.

46. Parsons, G.E., *et al.*, *Comparison of measured wetting behaviour of materials with identical surface energies, presented as particles and plates.* Journal of Adhesion Science and Technology, 1993. **7**(2): p. 95-104.

47. Chibowski, E. and R. Perea-Carpio, *Problems of contact angle and solid surface free energy determination.* Advances in Colloid and Interface Science, 2002. **98**: p. 245-264.

48. Chawla, A., *et al.*, *Wilhelmy plate contact angle data on powder compacts: considerations of plate perimeter.* European Journal of Pharmaceutical Sciences, 1994. **2**(3): p. 253-258.

49. Bilinski, B. and E. Chibowski, *The determination of the dispersion and polar free surface energy of quartz by the elution gas chromatography method.* Powder Technology, 1983. **35**: p. 39-45.

50. Planinsek, O., *et al.*, *The dispersive component of the surface free energy of powders assessed using inverse gas chromatography and contact angle measurements.* International Journal of Pharmaceutics, 2001. **221**(1-2): p. 211-217.

51. Mukhopadhyay, P. and H.P. Schreiber, *Aspects of acid-base interactions and use of inverse gas chromatography.* Colloids and Surfaces A: Physicochemical and Engineering Aspects, 1995. **100**: p. 47-71.

52. Balard, H., *et al.*, *Estimation of the surface energetic heteroneneity of fillers by inverse gas chromatography.* Macromolecular Symposia, 1996. **108**: p. 63-80.

53. Comard, M.-P.*, et al.*, *Inverse gas chromatographic study of the surface properties of talc impregnated with different acidic and basic polymers.* Powder Technology, 2002. **128**(2-3): p. 262-267.

54. Papirer, E.*, et al.*, *Inverse gas chromatography: a valuable method for the surface characterization of fillers for polymers (glass fibres and silicas).* European Polymer Journal, 1988. **24**(8): p. 783-790.

55. Ansari, D.M. and G.J. Price, *Correlation of the material properties of calcium carbonate filled polyproplylene with the filler surface energies.* Journal of Applied Polymer Science, 2003. **88**: p. 1951-1955.

56. Burry, W.M. and D.S. Keller, *Effects of dehydration on the apolar surface energetics of inorganic paper fillers.* Journal of Chromatography A, 2002. **972**(2): p. 241-251.

57. Fekete, E.*, et al.*, *Determination of the surface characteristics of particulate fillers by inverse gas chromatography at infinite dilution: a critical approach.* Journal of Colloid and Interface Science, 2004. **269**(1): p. 143-152.

58. Bandosz, T.J.*, et al.*, *Application of inverse gas chromatography to the study of the surface properties of modified layered minerals.* Microporous Materials, 1993. **1**: p. 73-79.

59. Hadjar, H.*, et al.*, *An inverse gas chromatography study of crystalline and amorphous silicas.* Colloids and Surfaces A: Physicochemical and Engineering Aspects, 1995. **99**(1): p. 45-51.

60. Pukanszky, B., *Influence of interface interaction on the ultimate tensile properties of polymer composites.* Composites, 1990. **21**(3): p. 255-262.

61. Pukanszky, B. and G. Voros, *Mechanism of interfacial interactions in particulate filled composites.* Composites Interfaces, 1993. **1**(5): p. 411-427.

62. Douillard, J.M.*, et al.*, *Surface Interactions between Silica Particles and Water and Organic Solvents.* Journal of Colloid and Interface Science, 1994. **164**(1): p. 238-244.

63. Douillard, J.M., *What Can Really Be Deduced from Enthalpy of Immersional Wetting Experiments?* Journal of Colloid and Interface Science, 1996. **182**(1): p. 308-311.

64. Douillard, J.M., *Immersion phenomena*, in *Interfacial Dynamics*, N. Kallay, Editor. 2000, Marcel Dekker: New York.

65. Malandrini, H., *et al.*, *Interactions between Talc Particles and Water and Organic Solvents.* Journal of Colloid and Interface Science, 1997. **194**(1): p. 183-193.

66. Bartell, F.E. and H.H. Zuidema, *Wetting characteristics of solids of low surface tension such as talc, waxes and resins.* Journal of the American Chemical Society, 1936. **58**(8): p. 1449-1454.

67. Fowkes, F.M. and W.D. Harkins, *The state of monolayers adsorbed at the interface solid-aqueous solution.* Journal of the American Chemical Society, 1940. **62**(12): p. 3377-3386.

68. Schrader, M.E. and S. Yariv, *Wettability of clay minerals.* Journal of Colloid and Interface Science, 1990. **136**(1): p. 85-94.

69. Yariv, S., *Wettability of Clay Minerals*, in *Modern Approaches to Wettability*, M.E. Schrader and I.L. George, Editors. 1992, Plenum Press: New York. p. 279-326.

70. Wu, W., *et al.*, *Change in surface properties of solids caused by grinding.* Powder Technology, 1996. **89**(2): p. 129-132.

71. Michot, L.J., *et al.*, *The structural microscopic hydrophilicity of talc.* Langmuir, 1994. **10**: p. 3765-3773.

72. Young, G.J., *et al.*, *Thermodynamics of the adsorption of water on graphon from heats of immersion and adsorption data.* Journal of Physical Chemistry, 1954. **58**: p. 313-315.

73. Chessick, J.J., *et al.*, *Adsorption and heat of wetting studies of teflon.* Journal of Physical Chemistry, 1956. **60**: p. 1345-1347.

74. Spagnolo, D.A., *et al.*, *Calculation of contact angle for hydrophobic powders using heat of immersion data.* Journal of Physical Chemistry, 1996. **100**: p. 6626-6630.

75. Yan, N., *et al.*, *Measurement of Contact Angles for Fumed Silica Nanospheres Using Enthalpy of Immersion Data.* Journal of Colloid and Interface Science, 2000. **228**(1): p. 1-6.

76. van Oss, C.J., *et al.*, *Determination of contact angles and pore sizes of porous media by column and thin layer wicking.* Journal of Adhesion Science and Technology, 1992. **6**(4): p. 413-428.

77. Washburn, E.W., *The dynamics of capillary flow.* The Physical Review, 1921. **17**(3): p. 273-283.

78. Bruil, H.G. and J.J. van Aarstsen, *The determination of contact angles of aqueous surfactant solutions on powders.* Colloid and Polymer Science, 1974. **252**: p. 32-38.

79. Crawford, R.*, et al.*, *Contact angles on particles and plates.* Colloids and Surfaces, 1987. **27**(1-3): p. 57-64.

80. Ku, C.A.*, et al.*, *Particle Transfer from a continuous oil to a dispersed water phase: model particle study.* Journal of Colloid and Interface Science, 1985. **106**(2): p. 377-387.

81. Holysz, L., *Surface free energy components of silica gel determined by the thin layer wicking method for different layer thicknesses of gel.* Journal of Materials Science, 1998. **33**: p. 445-452.

82. Bachmann, J.*, et al.*, *Development and application of a new sessile drop contact angle method to assess soil water repellency.* Journal of Hydrology, 2000. **231/232**: p. 66-75.

83. Bachmann, J.*, et al.*, *Modified sessile drop method for assessing initial soil-water contact angle of sandy soil.* Soil Sci Soc Am J, 2000. **64**(2): p. 564-567.

84. Drelich, J.*, et al.*, *Preparation of a coal surface for contact angle measurements.* Journal of Adhesion Science and Technology, 1997. **11**(11): p. 1399-1431.

85. *CRC Handbook of Chemistry and Physics*. 83 ed, ed. D.R. Lide. 2002: CRC Press.

86. Holysz, L., *The effect of thermal treatment of silica gel on its surface free energy components.* Colloids and Surfaces A: Physicochemical and Engineering Aspects, 1998. **134**(3): p. 321-329.

87. *FTA Drop shape analysis - user manual*. 2002.

88. Chibowski, E. and F. Gonzalez-Caballero, *Theory and practice of thin-layer wicking.* Langmuir, 1993. **9**: p. 330-340.

89. Chibowski, E., *Thin layer wicking - Methods for the determination of acid-base free energies of interaction*, in *Acid-base interactions: relevance to adhesion science and technology*, K.L. Mittal, Editor. 2000, VSP: Utrecht. p. 419-437.

90. Buckton, G., *Contact angle, adsorption and wettability -- a review with respect to powders.* Powder Technology, 1990. **61**(3): p. 237-249.

91. Douillard, J.M.*, et al.*, *Contact Angle and Film Pressure: Study of a Talc Surface.* Journal of Colloid and Interface Science, 2002. **255**(2): p. 341-351.

92. Hansford, D.T.*, et al.*, *The influence of processing variables on the wetting properties of a hydrophobic powder.* Powder Technology, 1980. **26**(2): p. 119-126.

93. Buckton, G.*, et al.*, *The effect of the comminution technique on the surface energy of a powder.* International Journal of Pharmaceutics, 1988. **47**(1-3): p. 121-128.

94. Buckton, G. and A.E. Beezer, *A microcalorimetric study of powder surface energetics.* International Journal of Pharmaceutics, 1988. **41**(1-2): p. 139-145.

95. Sheridan, P.L.*, et al.*, *The extent of errors associated with contact angles II. Factors affecting data obtained using a Wilhelmy plate technique for powders.* International Journal of Pharmaceutics, 1994. **109**(2): p. 155-171.

96. Kiesvaara, J. and J. Yliruusi, *The effect of compression time on the surface energy of tablets.* Acta Pharmaceutica Nordic, 1991. **3**(3): p. 171-177.

97. Zhang, D.*, et al.*, *Wettability of pharmaceutical solids: its measurement and influence on wet granulation.* Colloids and Surfaces A: Physicochemical and Engineering Aspects, 2002. **206**(1-3): p. 547-554.

98. Muster, T.H. and C.A. Prestidge, *Application of time-dependent sessile drop contact angles on compacts to characterise the surface energetics of sulfathiazole crystals.* International Journal of Pharmaceutics, 2002. **234**(1-2): p. 43-54.

99. Buckton, G.*, et al.*, *The extent of errors associated with contact angles 3. The influence of surface roughness effects on angles measured using a Wilhelmy plate technique for powders.* Colloids and Surfaces A: Physicochemical and Engineering Aspects, 1995. **95**(1): p. 27-35.

100. Stamm, A.*, et al.*, *Quantitative evaluation of the wettability of powders.* Drug Development and Industrial Pharmacy, 1984. **10**(3): p. 381-408.

101. Buckton, G., *Assessment of the wettability of pharmaceutical powders.* Journal of Adhesion Science and Technology, 1993. **7**: p. 205-219.

102. Parsons, G.E.*, et al.*, *The extent of the errors associated with contact angles obtained using liquid penetration experiments.* International Journal of Pharmaceutics, 1992. **82**(1-2): p. 145-150.